

**BGD**

10, 2705–2765, 2013

**Coastal  
thermo-erosion in the  
Laptev Sea**

F. Günther et al.

# Short and long-term thermo-erosion of ice-rich permafrost coasts in the Laptev Sea region

F. Günther<sup>1</sup>, P. P. Overduin<sup>1</sup>, A. V. Sandakov<sup>2</sup>, G. Grosse<sup>3</sup>, and M. N. Grigoriev<sup>2</sup>

<sup>1</sup>Alfred Wegener Institute Helmholtz Centre for Polar and Marine Research, Potsdam, Germany

<sup>2</sup>Permafrost Institute, Russian Academy of Sciences, Siberian Branch, Yakutsk, Russia

<sup>3</sup>Geophysical Institute, University of Alaska Fairbanks, Fairbanks, USA

Received: 19 January 2013 – Accepted: 29 January 2013 – Published: 15 February 2013

Correspondence to: F. Günther (frank.guenther@awi.de)

Published by Copernicus Publications on behalf of the European Geosciences Union.

Title Page

Abstract

Introduction

Conclusions

References

Tables

Figures



Back

Close

Full Screen / Esc

Printer-friendly Version

Interactive Discussion



## Abstract

Permafrost coasts in the Arctic are susceptible to a variety of changing environmental factors all of which currently point to increasing coastal erosion rates and mass fluxes of sediment and carbon to the shallow arctic shelf seas. Rapid erosion along high yedoma coasts composed of Ice Complex permafrost deposits creates impressive coastal ice cliffs and inspired research for designing and implementing change detection studies for a long time, but continuous quantitative monitoring and a qualitative inventory of coastal thermo-erosion for large coastline segments is still lacking. Our goal is to use observations of thermo-erosion along the mainland coast of the Laptev Sea in eastern Siberia to understand how erosion rates depend on coastal geomorphology and the relative contributions of waterline and atmospheric drivers to coastal thermo-erosion over the past 4 decades and in the past few years. We compared multitemporal sets of orthorectified satellite imagery from 1965 to 2011 for three segments of coastline with a length of 73 to 95 km each and analyzed thermo-denudation (TD) along cliff top and thermo-abrasion (TA) along cliff bottom for two nested time periods: long-term rates (the past 39–43 yr) and short term rates (the past 1–3 yr). The Normalized Difference Thermo-erosion Index (NDTI) was used as a proxy that qualitatively describes the relative proportions of TD and TA. Mean annual erosion rates at all three sites were higher in recent years ( $-5.3 \pm 1.31 \text{ m a}^{-1}$ ) than over the long term mean ( $-2.2 \pm 0.13 \text{ m a}^{-1}$ ). The Mamontov Klyk coast exhibit primarily spatial variations of thermo-erosion, while intrasite-specific variations were strongest at the Buor Khaya coast, where slowest long-term rates around  $-0.5 \pm 0.08 \text{ m a}^{-1}$  were observed. The Oyogos Yar coast showed continuously rapid erosion up to  $-6.5 \pm 0.19 \text{ m a}^{-1}$ . In general, variable characteristics of coastal thermo-erosion were observed not only between study sites and over time, but also within single coastal transects along the cliff profile. Varying intensities of cliff bottom and top retreat are leading to diverse qualities of coastal erosion that have different impacts on coastal mass fluxes. The different extents of Ice Complex permafrost degradation within our study sites turned out to

BGD

10, 2705–2765, 2013

### Coastal thermo-erosion in the Laptev Sea

F. Günther et al.

Title Page

Abstract

Introduction

Conclusions

References

Tables

Figures

◀

▶

◀

▶

Back

Close

Full Screen / Esc

Printer-friendly Version

Interactive Discussion



influence not only the degree of coupling between TD and TA, and the magnitude of effectively eroded volumes, but also the quantity of organic carbon released to the shallow Laptev Sea from coastal erosion, which ranged on a long-term from  $88 \pm 21.0$  to  $800 \pm 61.1$  t per km coastline per year and will correspond to considerably higher amounts, if recently observed more rapid coastal erosion rates prove to be persistent.

## 1 Introduction

Coastal erosion as a physical process along the marginal arctic shelf seas attracts increased attention not only in periglacial research (e.g. Lantuit et al., 2011b; Vasiliiev et al., 2011), marine geosciences (Charkin et al., 2011), but also in the public awareness in terms of rapid responses of coastal erosion to climate warming, leading to landscape instability and increased hazard exposure (Forbes, 2011). Because of recently decreasing sea ice extent (Comiso et al., 2008; Maslanik et al., 2011), larger fetch (Asplin et al., 2012), wave action and storm activity (Jones et al., 2009), a doubling in the duration of the open water season (Overeem et al., 2011), and rising air, permafrost, and sea water temperatures during the last decades (Romanovsky et al., 2010; Dmitrenko et al., 2011; AMAP, 2011), erosion of arctic permafrost coasts and land loss are expected to increase. The enhanced material fluxes in the nearshore zone, including sediment, organic matter, and nutrients, affect marine ecosystems and primary production in arctic coastal habitats (Wassmann, 2011). The Arctic Ocean is the most land-dominated ocean basin, because of its large continental catchments (Peterson et al., 2002), where terrigenous dissolved organic carbon is mobilized from high latitude carbon-rich soils and peatlands (Benner et al., 2004). Permafrost affected arctic coasts make up approximately 34 % of the world's coastlines (Lantuit et al., 2011b), and feature an unique suite of coastal processes with strong seasonality, cold temperatures, permafrost, and sea ice, found nowhere else except Antarctica (Forbes, 2011). In the Laptev Sea region, 25 % of the 7500 km long coastline are composed of very

**BGD**

10, 2705–2765, 2013

## Coastal thermo-erosion in the Laptev Sea

F. Günther et al.

Title Page

Abstract

Introduction

Conclusions

References

Tables

Figures

◀

▶

◀

▶

Back

Close

Full Screen / Esc

Printer-friendly Version

Interactive Discussion



ice-rich permafrost deposits (Grigoriev et al., 2006), which are highly susceptible to erosion.

In many regions, the coastal zone of the shallow East Siberian Arctic Shelf has a dominantly heterotrophic character (Pipko et al., 2011), where organic and inorganic carbon from coastal erosion and river runoff result in sea acidification and out-gassing of CO<sub>2</sub> to the atmosphere (Razumov and Grigoriev, 2011). In addition, Are (1999) and Rachold et al. (2000) find that sediment release to the ocean from the coasts in the Laptev Sea region is at least of the same order of magnitude as the amount of riverine input, underlining the importance of coastal erosion processes and the need for better quantification.

Along permafrost-dominated coasts, heat transfer and melt of ground ice is added to the mechanical erosion forces of waves and ice. This process of thermo-erosion dominates the majority of the Laptev Sea coast (Fig. 1) and leads to rapid erosion rates and the subsequent inundation of continental polygenetic permafrost deposits (Winterfeld et al., 2011), including the Ice Complex (in Russian “ledovyi kompleks”; also called yedoma) and thermokarst (also called alas) deposits (e.g. Schirrneister et al., 2011b). Geomorphologically, yedoma constitutes hilly uplands and alas low lying basins, establishing local differences in elevation, e.g. up to 27 m in the Lena Delta (Ulrich et al., 2010). Both types of deposits also contain high amounts of ground ice and soil organic carbon (Schirrneister et al., 2011a; Strauss et al., 2012), making them generally very vulnerable to carbon mobilization from disturbances (e.g. Grosse et al., 2011), especially in coastal settings (Grigoriev et al., 2004; Semiletov et al., 2011).

Thermo-erosion creates coastal cliffs with geomorphological features unique to ice-rich coastlines. Two mass transport processes that combine thermal and mechanical forces to erode the coastline are thermo-denudation (TD) thermo-abrasion (TA) (see Are, 1988a,b; Dupeyrat et al., 2011, and Fig. 2). TA is defined as the combined mechanical and thermal effects of impinging wave energy at the shoreline. TD is defined as the combined influence of solar insolation and heat advection, influencing the energy balance at the ground surface above the waterline, and can be conceived as periglacial

**BGD**

10, 2705–2765, 2013

## Coastal thermo-erosion in the Laptev Sea

F. Günther et al.

Title Page

Abstract

Introduction

Conclusions

References

Tables

Figures



Back

Close

Full Screen / Esc

Printer-friendly Version

Interactive Discussion



coastal landslides. As an agent of TD, melt water from ground ice causes water saturation on coastal slopes, enabling gelifluction of blocks and mud stream development. In addition to erosion products resulting from TA, TD on coastal cliffs delivers eroded clastic material to the cliff's bottom edge and to the shore platform. Often, additional processes such as thermo-niche development and mechanical failure of ice-wedge polygonal blocks along eroding coasts enhance mass transport rates. We adopt the definition of thermo-erosion of the permafrost coast of Are (1988a) as the combined effects of TD and TA.

Ice Complex coasts have been studied by other researchers. For instance, Kaplina (1959) describes acceleration of coastal erosion in connection with the occurrence of large ice wedge bodies, leading to a reduction of material accruing during undercutting of coastal cliffs through thermo-niches. Klyuev (1970) carries out repeated surveys to quantify thermo-abrasion of the sea bottom. Are et al. (2005) develop a method for calculating coastal retreat rate based on the dimensions of thermo-terraces widespread across the Laptev Sea coast. Overduin et al. (2007) present a conceptual model of permafrost preservation under submarine conditions in dependence on coastal erosion rates. Grigoriev (2008) does monitoring and analytical work on coastal permafrost dynamics and mass fluxes on the East Siberian Arctic Shelf. Razumov (2010) systemizes endogeneous and exogeneous factors for modelling approaches of permafrost coastal erosion. Recent contributions are conducted by Pizhankova and Dobrynina (2010) and Lantuit et al. (2011a), who carry out remote sensing time series analyses of coastal erosion dynamics for the entire Lyakhov Islands and the Bykovsky Peninsula, respectively.

The Arctic Coastal Dynamics Project (ACD) (Rachold et al., 2003) and Lantuit et al. (2011b) report a weighted mean annual coastal erosion rate for the Laptev Sea of  $0.73 \text{ m per year}$  ( $\text{ma}^{-1}$ ). Grigoriev (2008) quantify a mean retreat rate of  $1.9 \text{ ma}^{-1}$ , for coastal segments containing Ice Complex deposits. Usually, these values come from a variety of data sources, such as rare field surveys with high temporal frequency and comparison of historical aerial photographs with geodetic measurements (Grigoriev

## BGD

10, 2705–2765, 2013

### Coastal thermo-erosion in the Laptev Sea

F. Günther et al.

Title Page

Abstract

Introduction

Conclusions

References

Tables

Figures

◀

▶

◀

▶

Back

Close

Full Screen / Esc

Printer-friendly Version

Interactive Discussion



et al., 2003, 2009; Grigoriev, 2008). Studies on coastal erosion in the eastern sector of the Russian Arctic are spatially limited and inconsistent in their methods of data collection and interpretation. Therefore, satellite-based remote sensing offers the only viable mean of observing, quantifying and monitoring coastal erosion dynamics in the Arctic over large regions. Although the morphodynamics of permafrost coasts have been investigated in various regions, the relative intensities and contributions of TD and TA to erosion dynamics require detailed quantitative study. Despite the existence of absolute long-term and actual coastal retreat rates, adequate interpretation will depend on analyzing which processes drive local thermo-erosion.

The objective of this paper is to use observations of thermo-erosion along the Laptev Sea coastline to understand the relative contributions of TD and TA to the erosion of ice-rich permafrost coasts over the past four decades and over the past few years, in three different settings in the Laptev Sea region. We apply the concept of Normalized-Difference-Thermo-erosion-Index (NDTI) of Günther et al. (2012), as a dimensionless index of the ratio of TD and TA above the waterline. Using state-of-the-art digital image processing and GIS change detection techniques, we determine and compare mean annual coastal erosion rates for long and short-term observation periods. Using our findings, we discuss the impacts of these permafrost degradation processes on mass fluxes of organic carbon from land to arctic shelf sea. Understanding spatial patterns of thermo-erosion and how associated processes change over time will help us gain predictive capability as conditions for erosion in the Arctic are changing.

## 2 Study site description

### 2.1 Geographical setting

All studied sites are located in northern Yakutia (Russian Federation) along the mainland coast of the Laptev Sea that extends from Taymir in the west to Cape Svyatoi Nos at the transition to the East Siberian Sea (Fig. 1). According to Treshnikov

**BGD**

10, 2705–2765, 2013

## Coastal thermo-erosion in the Laptev Sea

F. Günther et al.

Title Page

Abstract

Introduction

Conclusions

References

Tables

Figures

⏪

⏩

◀

▶

Back

Close

Full Screen / Esc

Printer-friendly Version

Interactive Discussion



(1985), the territories of the outermost sites Mamontov Klyk and Oyogos Yar belong to the Arctic tundra, the Buor Khaya Peninsula to the northern tundra zone. The sub-arctic climate is continental and characterized by long harsh winters and short cold summers. Mean annual air temperature in Tiksi in the southern central Laptev Sea is  $-11.5^{\circ}\text{C}$  (Romanovsky et al., 2010), the amplitude of seasonal variation  $40.6^{\circ}\text{C}$  (Kholodov et al., 2012). Terrestrial permafrost is continuously distributed in the region (Popov, 1989). The Laptev Sea is one of the shallow Siberian shelf seas (Fig. 1) and is underlain by subsea permafrost up to 500–650 m deep along the mainland coast (Romanovskii and Tumskey, 2011). Roughly from October to June, the coastal sea is covered by thick one-year land fast sea ice. The sea ice-free season lasts for only 14 % in the western, and 20 % of the year in the eastern Laptev Sea (Dunaev and Nikiforov, 2001). The Olenyok-Anabar and Yana-Indigirka coastal lowlands (Fig. 1) in the North of East Siberia represent former late Pleistocene accumulation plains. Subjected to permafrost degradation processes, nowadays their geomorphology is determined by levelling through thermokarst and drainage development in direction to the coast. By far the largest river in the Laptev Sea region is the Lena River with an annual water discharge of  $529 \text{ km}^3$  (ROSHYDROMET and ArcticRIMS, 2009).

The Laptev Sea region is a unique geodynamic system, where active mid-oceanic seafloor spreading transforms into a passive rift system on continental crust (Sekretov, 2001), characterized by an alternating syncline-anticline system of neotectonic uplifted horsts and small grabens (Drachev et al., 1998). A variation of the coastal morphology in the Siberian Arctic is influenced by glacial isostatic adjustment during the Holocene (Whitehouse et al., 2007). West and Middle Siberian rivers terminate in estuaries, while East Siberian rivers form marine deltas. According to Whitehouse et al. (2007) the transition between these two types of drainage occurs approximately at longitude  $115^{\circ}\text{E}$ . This is the western starting point of our study site transect along the Laptev Sea mainland coast.

**BGD**

10, 2705–2765, 2013

## Coastal thermo-erosion in the Laptev Sea

F. Günther et al.

Title Page

Abstract

Introduction

Conclusions

References

Tables

Figures

◀

▶

◀

▶

Back

Close

Full Screen / Esc

Printer-friendly Version

Interactive Discussion



## 2.2 Mamontov Klyk

The studied coastline in the western Laptev Sea between the estuary of the Anabar River and the Olenyok River delta extends from Cape Lygi across Cape Mamontov Klyk to the former polar station at Cape Terpyai Tumus in the East (Fig. 1; 73° 41' 45" N 115° 53' 7" E and 73° 33' 11" N 118° 42' 16" E). According to Schirrmeister et al. (2008) the stratigraphy of the permafrost sequences cropping out at the coast cover late Pleistocene and Holocene strata and is composed of less ice-rich fluvial silts and sands with peat layers, covered with 20–30 m thick ice-supersaturated silty to sandy Ice Complex deposits. Holocene thermokarst deposits have been found in alluvial, thermoerosional valleys and in places discordantly superimposing the Ice Complex (Grosse et al., 2006). The hinterland of the coast is gently inclined towards the Laptev Sea coast in the north with a mean slope of 0.1° and incised by a dendritic network of thermo-erosional valleys (Schirrmeister et al., 2008). Coastline length between the end points in this study near capes Lygi and Terpyai Tumus is 95 km, 56 km of which are studied for coastal dynamics. The remaining part of the coastline consists of river mouths with small deltaic accumulation cones, alluvial marshy bays, and marine terraces and sand spits, without visible erosion (e.g. Fig. 2). Although the coastline is generally straightened by thermo-abrasion, it features a wavy pattern with convex protrusions and concave indentations on a mesoscale of tens of kilometers. Klyuev (1970) describes alongshore coastal material drift from west to east for this region, resulting in the large sand accumulation zone at the outer margin of Terpyai Tumus. The high ground ice volume renders this coastline exceptionally well suited to high cliff retreat rates.

## 2.3 Buor Khaya

The central study site is the western coast of the Buor Khaya Peninsula (Fig. 1). Bordered by two grabens that dissipated north of the Buor Khaya Cape (Imaeva et al., 2007), the peninsula is part of the Yana-Omoloi interfluvium and an uplifted block. According to Strauss and Schirrmeister (2011), outcrops of Ice Complex and alas deposits in

BGD

10, 2705–2765, 2013

### Coastal thermo-erosion in the Laptev Sea

F. Günther et al.

Title Page

Abstract

Introduction

Conclusions

References

Tables

Figures

◀

▶

◀

▶

Back

Close

Full Screen / Esc

Printer-friendly Version

Interactive Discussion



5 this region consist of silty fine sand with peaty inclusions. The western coastline of the Buor Khaya Peninsula reveals a high heterogeneity of geomorphological units, such as tapped lake basins, alasses (9–14 m above mean sea level (a.m.s.l.)), yedoma hills (up to 37 m a.m.s.l.) and transition zones between the latter two. The hinterland is inclined  
10 towards north with a mean slope of  $0.05^\circ$ , and is characterized by thermokarst relief. Isolated yedoma remnants cover only 15 % of the area, which are dissipated by coalesced thermokarst basins. Dunaev and Nikiforov (2001) describe alongshore material drift from south to north, manifested in the 30 km long Buor Khaya spit, the product of littoral processes. The length of the Buor Khaya west coast between the outermost points  
15 of this study ( $71^\circ 20' 41''$  N  $132^\circ 3' 23''$  E and  $71^\circ 56' 49''$  N  $132^\circ 45' 44''$  E) is 73 km, of which 48 km were studied for coastal erosion dynamics.

## 2.4 Oyogos Yar

15 The third study region belongs to the Yana-Indigirka lowland and extends along the Oyogos Yar mainland coast of the Dmitry Laptev Strait from Cape Svyatoi Nos in the West to the Kondratyeva River mouth in the East (Fig. 1). Cape Svyatoi Nos is an isolated cretaceous granite dome (433 m a.m.s.l.), where the beach of the rocky coast is characterized by large sized boulders (Are et al., 2002). In the vicinity of Svyatoi Nos, yedoma hills with Ice Complex remnants are degraded by closely spaced thermo-erosional valleys, become less frequent further east and are again found at the outer  
20 eastern margin of the coastline segment. The stratigraphy at the Oyogos Yar coast includes Eemian lacustrine deposits followed by late Pleistocene Ice Complex deposits as well as Holocene thermokarst sequences (Wetterich et al., 2009). Most of the coast cuts through thermokarst depressions. According to Opel et al. (2011), alas bottoms reach elevations of about 8–12 m a.m.s.l. and consist of poorly sorted silt with peat inclusions and syngenetic ice wedges. The very gently inclined steplike landscape inland  
25 (Schirrmeister et al., 2011b) is drained by several thermoerosional valleys. The direction of surface currents in the Dmitry Laptev Strait, the gateway to the East Siberian Sea, is from west to east. The length of the observed coastline (between  $72^\circ 46' 59''$  N

## Coastal thermo-erosion in the Laptev Sea

F. Günther et al.

Title Page

Abstract

Introduction

Conclusions

References

Tables

Figures



Back

Close

Full Screen / Esc

Printer-friendly Version

Interactive Discussion



141° 30' 51" E and 72° 39' 20" N 143° 50' 36" E) is 81 km, all of which are included in this analysis.

### 3 Methods

#### 3.1 Remote sensing data fusion approach

5 In order to provide a consistent picture of coastal erosion rates for our study sites, we applied a common best-practice strategy of data collection, fusion, examination and analysis to all three sites. Accurate monitoring of coastline changes using multi-temporal, multi-platform remotely sensed data requires consideration of various distortions, including distortions associated with the platform, the map projection, and shape of the Earth's surface. In this study we use high and very high spatial resolution CORONA KH-4A and KH-4B, ALOS PRISM, KOMPSAT-2, SPOT-5, RapidEye and GeoEye space-borne imagery with differing geometric characteristics (Tables 1, 2, and 3). For coastline digitalization we used images of similar high spatial resolution (0.5–2.5 m). All images used were acquired at different times, and at different oblique viewing and azimuth angles.

15 Conventional 2-D polynomial image rectification functions for image co-registration do not correct for relief induced and image acquisition system distortions. Toutin (2004) points out that 2-D ground control points (GCPs) correct for local distortions at the GCP location and are very sensitive to input errors. Consequently, this approach should be avoided for precise geometric multi-source/multi-format data integration. Our object of interest, the coastline, is always outside a cloud of GCPs on land. Therefore, the accuracy of our measurements relies heavily on correct terrain approximation and physical sensor models, since all images used are off-nadir.

### 3.2 Georeferencing and ortho-rectification

Registration of multiple source imagery is one of the most important issues when dealing with remote sensing data (Le Moigne et al., 2011). Change detection over time requires multitemporal data calibration through georeferencing, that is explicit assignment of geodata with absolute position information of a co-ordinate system. The initial georeferencing basis for multispectral optical GeoEye and RapidEye image data is a network of GPS GCPs of well identifiable immobile features, such as small ponds, collected in the field. The GCPs which were incorporated into the tachometric surveys are known with high absolute accuracy of  $\leq 1$  m. Other single GCPs were collected in the field using the GPS waypoint averaging function to achieve good positional accuracy of 2–4 m. Polygon ponds studied by Wetterich and Schirrmeyer (2008), served as GCPs in the Oyogos Yar region. This selection of GCPs was then localized in the imagery and used for manual image registration. The potential georeferencing accuracy improves when ground resolution of the imagery increases. With the aid of additional parameter models as Fraser and Ravanbakhsh (2009) describe, georeferencing of GeoEye imagery (Geo & GeoStereo level) showed very good results, often with sub-metre accuracy. For areas with no GeoEye coverage, RapidEye serves as master dataset for further registration purposes. Having RapidEye (Level 1B) wide area imagery that come with the full internal and external orientation parameters and rational polynomial coefficients (RPC), we were able to filter out inaccurate GCPs and to establish for all sites a common and comparable high resolution reference data set with large areal coverage and absolute root mean square errors (RMSE  $\delta_a$ ) within pixel size (Tables 1, 2, and 3). It was used as a basis of equal quality for georeferencing all imagery for long-term observations, covering areas where no direct ground survey data were available. All input and reference scenes were projected using the respective UTM zone (50N, 53N and 54N) on a WGS-84 model.

CORONA imagery may serve as a substitute for historic aerial imagery in north-east Siberia since it provides high ground resolution (2–3 m) and a historical record

BGD

10, 2705–2765, 2013

#### Coastal thermo-erosion in the Laptev Sea

F. Günther et al.

Title Page

Abstract

Introduction

Conclusions

References

Tables

Figures



Back

Close

Full Screen / Esc

Printer-friendly Version

Interactive Discussion



## Coastal thermo-erosion in the Laptev Sea

F. Günther et al.

Title Page

Abstract

Introduction

Conclusions

References

Tables

Figures



Back

Close

Full Screen / Esc

Printer-friendly Version

Interactive Discussion



for observing long-term changes, (Grosse et al., 2005). A challenging task is the rec-  
tification of panoramic CORONA KH-4A and KH-4B imagery for mapping purposes. Sohn et al. (2004) describe several distortion overlap effects, which are maximized to-  
wards the ends of each photograph. Fragments of our sites lie at the margins of the  
film strips and are therefore strongly affected by perspective distortions. Following Piec-  
zonka et al. (2011), we use Remote Sensing Graz (RSG, 2011) software for processing  
CORONA data of the years 1965, 1968, and 1969, which were obtained from the U.S.  
Geological Survey as four image tiles at 7  $\mu\text{m}$  scan resolution. Stitching image tiles  
and subsequent subsetting of a region of interest was done in Adobe<sup>®</sup> Photoshop<sup>®</sup>  
CS5.5, to retain the subset position within the full film strip dimensions. Using RSG  
with an implemented parametric sensor model, we were able to reconstruct inner and  
outer orientation parameters of the image acquisition in order to calculate the effective  
ground resolution of each subset. The geometric resolution ( $\delta_p$ ) in m of each CORONA  
subset was calculated from:

$$\delta_p = \frac{h}{c_k} \cdot \Delta\eta_s \quad (1)$$

where  $h$  is flight height,  $c_k$  focal length, and  $\eta_s$  digitizing distance. Ground resolu-  
tion ranged from 2.0 to 2.9 m (Tables 1, 2, and 3). Neighboring and laterally overlap-  
ping scenes we handled as joint photogrammetric image blocks for subsequent ortho-  
rectification. For mapping purposes within ortho-images, the scenes of the CORONA  
AFT (backward looking) camera were preferred, as the CORONA FWD (forward look-  
ing) camera scenes showed either lower radiometric quality or less favourable overlap  
situation. We ortho-rectified CORONA data using digital elevation models (DEMs) cre-  
ated from CORONA along-track stereoscopic images acquired at the same time (Ma-  
montov Klyk study site), from topographic maps with an contour equidistance of 10 m  
that were produced based on aerial surveys from 1973 (Buor Khaya study site), or  
from several ellipsoid-based ortho-image series using sea level or varying cliff heights  
as a basis (Oyogos Yar) with regard to coastal cliff bottom and top line delineation.

## Coastal thermo-erosion in the Laptev Sea

F. Günther et al.

Title Page

Abstract

Introduction

Conclusions

References

Tables

Figures



Back

Close

Full Screen / Esc

Printer-friendly Version

Interactive Discussion



The Panchromatic Remote-Sensing Instrument for Stereo Mapping (PRISM) on board the Advanced Land Observing Satellite (ALOS) had a forward, backward, and nadir channel. They formed an along-track triplet scene with 2.5 m resolution. We corrected PRISM data (Level 1B1) from 2007 and 2009 for the Mamontov Klyk study site using DEM's that we generated from triplets (OBS1 data) and stereo scenes of backward and nadir looking scenes (OBS2 data). Prior to DEM extraction and orthorectification we reduced JPEG noise from PRISM data using the software of Kamiya (2008). Panchromatic data obtained by SPOT5-HRS (High Resolution Stereoscopic), provided also imagery at comparable ground resolution of 2.5 m. We corrected SPOT-5 data (Level 1A) for Buor Khaya and Oyogos Yar using DEMs that we generated from 1-day interval across-track stereo pairs of the same datasets. In combination with the CORONA datasets, PRISM and SPOT-5 data span our long-term observation periods of several decades up to 43 yr.

To determine recent short-term coastal erosion rates we used a time series of multiple GeoEye and KOMPSAT-2 very high resolution images. In case of a spatial overlap, these images were geo-referenced to each other, making it easier to find common GCPs close to the coastline. We applied pan-sharpening (Ehlers et al., 2010) to all KOMPSAT-2 and GeoEye-1 imagery, used for short-term measurements. All processing of recent remote sensing data was done using PCI Geomatic's<sup>®</sup> Geomatica 2012 OrthoEngine.

### 3.3 Field work

Field sites were surveyed during joint Russian-German expeditions “Eastern Laptev Sea – Buor Khaya Peninsula 2010” (Wetterich et al., 2011) and “Western Laptev Sea – Mamontov Klyk 2011”. During field work we produced a basic dataset of precise topographic reference measurements for better interpretation of remote sensing products, to improve classification of coastal relief units and as input for the creation of large-area DEMs. Our geodetic measuring setup using a ZEISS ELTA C30 tacheometer and corresponding reflector mirrors is described in detail by Günther et al. (2011). A total of

6.7 km coastline distributed over six key sites was surveyed on Buor Khaya, and 2.1 km around Cape Mamontov Klyk. No measurements were made at Oyogos Yar. However, for this site we rely on existing literature about the Dmitry Laptev Strait region, which has been the subject of research on permafrost deposits (Wetterich et al., 2009), on the formation of subsea permafrost (Grigoriev, 2008), disappearing islands (Gavrilov et al., 2003) and coastal erosion (Pizhankova and Dobrynina, 2010).

### 3.4 Coastline digitalization

Cliff bottom and cliff top coastlines were manually digitalized separately using ESRI® ArcGIS™ 10 software. Delineating the same section of shoreline at different spatial scales results in different coastline lengths and therefore also different volumes for sediment flux (Lantuit et al., 2009). Depending on the complexity of the coastline and on-screen specific image contrast we used fine mapping scales from 1 : 500 to 1 : 2000 in this study. We used the Digital Shoreline Analysis System (DSAS) of Thieler et al. (2009), available as an extension to ArcGIS™, to calculate shoreline position changes between two dates, a method previously used for example for assessing coastal erosion on the Beaufort Sea coast (Jones et al., 2009) as well as thermokarst lake shore erosion on the Seward Peninsula in Alaska (Jones et al., 2011). An arbitrary baseline located offshore and following the coastline was created by buffering the oldest seaward-most coastline, 100 m off the coast. Every 50 m along this baseline, transects perpendicular to the coastline were used for separate determination of cliff bottom and cliff top line retreat, regarded as TA and TD, respectively (Fig. 2). With the aid of DEM's and all available imagery, we visually classified transects as either yedoma hill or alas basin. Coastal retreat was measured as absolute displacement distance metrics over a known period of time. Therefore, coastal erosion rate was calculated using:

$$r = \frac{-1 \cdot (x_1 - x_2)}{t_1 - t_2} \quad (2)$$

**BGD**

10, 2705–2765, 2013

## Coastal thermo-erosion in the Laptev Sea

F. Günther et al.

Title Page

Abstract

Introduction

Conclusions

References

Tables

Figures

◀

▶

◀

▶

Back

Close

Full Screen / Esc

Printer-friendly Version

Interactive Discussion



where  $x_1$  and  $x_2$  are coastline positions relative to the baseline at times  $t_1$  and  $t_2$ . The factor of  $-1$  is used in order to define erosion as negative.

### 3.5 Uncertainty assessment

Uncertainty in planimetric coastline positions has numerous sources. To limit geometric distortions, we work with a geometrically consistent dataset of ortho-images. To quantify uncertainties we consider:

1. georeferencing to an absolute frame of a coordinate system ( $\delta_a$ ),
2. relative georeferencing of two data sets to each other ( $\delta_r$ ),
3. the geometric resolution of the data set ( $\delta_p$ ) and
4. relief-induced horizontal displacement as a result of ortho-rectification ( $\delta_z$ ).

The sources of uncertainty  $\delta_a$  and  $\delta_r$  depend on the method of image to image georeferencing. Data sets used for long-term measurements are referenced to a common reference data set, where the reference itself is not used for measurements. Here the georeferencing uncertainty is the geometric mean of the RMS errors  $\delta_r$  and  $\delta_a$  for each data set. For short-term measurements we neglect  $\delta_a$  of the initial reference data set, because for relative coastline positions derived from second order derivatives of data processing the respective referencing basis provides itself a coastline position. That means, for data sets geo-referenced to each other,  $\delta_r$  is the RMS error of the mutual georeferencing. The uncertainty deriving from the spatial resolution of the data set is taken to be half of the spatial resolution.  $\delta_z$  arises out of a combination of errors in topographic approximation and the tilt angle associated with oblique image data acquisition, where both are unique to and are calculated from the underlying DEM data set. Relief-induced error is calculated from:

$$\delta_z = \tan \alpha \cdot \Delta z \quad (3)$$

where  $\alpha$  is the tilt angle of the spacecraft and  $\Delta z$  the vertical accuracy of the DEM. The cumulative uncertainty in coastline position for long-term measurements is then given by the quadratic sum:

$$\delta x = \sqrt{\left(\sqrt{\delta_a^2 \cdot \delta_r^2}\right) + \delta_p^2 + \delta_z^2} \quad (4)$$

and for short-term measurements accordingly by:

$$\delta x = \sqrt{\delta_r^2 + \delta_p^2 + \delta_z^2} \quad (5)$$

The cumulative uncertainty in coastline position is given as  $\delta x_1$  and  $\delta x_2$  for positions at times  $t_1$  and  $t_2$ , respectively. Uncertainties for acquisition times ( $t$ ) are less than 0.01 % and are neglected. Assuming that the cumulative uncertainties in coastline position are random and independent, we calculate uncertainty in coastline position change rate as:

$$\delta r = \frac{\sqrt{\delta x_1^2 + \delta x_2^2}}{t_1 - t_2} \quad (6)$$

Uncertainties in change rate calculation may also arise from the discrepancy between taking the continuous time range between two dates as a basis or the factual ice-free period of time. This effect applies for detection of short term changes and especially for comparison of those between the study sites.

### 3.6 Normalized Difference Thermo-erosion Index (NDTI)

Since we aim at evaluating spatial patterns of thermo-erosion, we did not quantify shore sections dominated by accumulation. Based on our multitemporal remote sensing data stable coasts included segments with extensive beaches and segments with inactive

**Coastal thermo-erosion in the Laptev Sea**

F. Günther et al.

Title Page

Abstract

Introduction

Conclusions

References

Tables

Figures



Back

Close

Full Screen / Esc

Printer-friendly Version

Interactive Discussion



cliffs that did not change within our measurement uncertainties of a particular transect. Along segments where a cliff position was blurred, i.e. by undisturbed vegetation cover, we did not track cliff positions over time.

For ice-rich permafrost coasts, we assume that movement of the top of the coastal cliff is attributable to TD, and the movement of the cliff bottom is attributable to TA, as defined above (Fig. 2). Different relative intensities of these two processes create a large variety of coastal slope profiles (Sovershaev, 1992) and must be considered in measurements. Here, we apply the concept of the Normalized Difference Thermo-erosion Index (NDTI) of Günther et al. (2012), that qualitatively describes the shape of coastal change and as a proxy allows for interpretation of planimetric erosion rates. NDTI is calculated from:

$$\text{NDTI} = \frac{\text{thermodenudation} - \text{thermoabrasion}}{\text{thermodenudation} + \text{thermoabrasion}} = \frac{\text{TD} - \text{TA}}{\text{TD} + \text{TA}} \quad (7)$$

TD and TA values in the equation can be either absolute shoreline movement or rates over time. As a ratio of two numbers which have the same units, NDTI is a dimensionless quantity. NDTI values range from  $-1$  (only TA) to  $+1$  (only TD). Weaknesses of the NDTI approach are outlined in Günther et al. (2012) and mostly comprise the missing consideration of thermo-erosional niche development.

## 4 Results

### 4.1 Coastal thermo-erosion at Mamontov Klyk

Along the western study site coast mean long-term TD and TA both were  $-2.1 \text{ ma}^{-1}$  with a standard deviation of  $\pm 1.2$ . The Mamontov Klyk coast features low, medium, and high coastal erosion rates with nearly equal frequency (Fig. 3), except for very rapid rates ( $\leq 3.5 \text{ ma}^{-1}$ ). Differentiation of coastal erosion into TD and TA shows a bimodal distribution of all long-term TD and TA values, which reflects the spatial variability of

**BGD**

10, 2705–2765, 2013

## Coastal thermo-erosion in the Laptev Sea

F. Günther et al.

Title Page

Abstract

Introduction

Conclusions

References

Tables

Figures

◀

▶

◀

▶

Back

Close

Full Screen / Esc

Printer-friendly Version

Interactive Discussion



thermo-erosion along the whole coastline. Coastal erosional patterns along the Mamontov Klyk coast exhibit a break in west-east direction (Fig. 4). From Cape Lygi in the west, to the Urasalakh River mouth, mean TD and TA were  $-1 \text{ ma}^{-1}$ , while coastline sections further east around capes Mamontov Klyk and Terpyai Tumus had TD and TA values around  $-2.9 \text{ ma}^{-1}$  and  $-2.5 \text{ ma}^{-1}$ , respectively. Numerous regional sediment traps and non-eroding stable segments are interspersed among eroding segments of the Mamontov Klyk coast. The highest observed long-term TD rates on Mamontov Klyk yedoma coasts were about  $-5.7 \text{ ma}^{-1}$ , which was not necessarily connected with TA rates of the same order, while TD and TA rates for alas coasts were proportional to each other (Fig. 5). Although measurements of TD and TA rates on Mamontov Klyk exhibit the strongest correlation ( $r^2 = 0.68$ ) for yedoma across all three study sites, they lagged behind the high correlation of TD and TA along alas coasts ( $r^2 = 0.95$ ). On the Mamontov Klyk coast, we observed the least variation in coastal erosion rates between different coastline types, where TD and TA rates for alas are in the range of only 10–15% lower than for yedoma transects. NDTI data revealed long-term values of 0.14 and  $-0.12$  for TD and TA dominated coasts, respectively. Figure 6 shows an equal distribution of NDTI for the Mamontov Klyk coast, where TA is observed slightly more frequently.

The temporal variability of coastal erosion rates along the Mamontov Klyk coast is reflected in recently more rapid mean TD ( $-4.5 \text{ ma}^{-1} \pm 1.2$ ) and mean TA short-term rates ( $-4.6 \text{ ma}^{-1} \pm 1.2$ ), compared to long-term observations of  $-2.8 \text{ ma}^{-1}$  and  $-2.9 \text{ ma}^{-1}$ , respectively (Fig. 7). Most outliers ( $\geq -21 \text{ ma}^{-1}$ ) are to more rapid erosion events (rather than slower) of TD in short-term measurements at capes Mamontov Klyk and Terpyai Tumus. Short-term NDTI values have a broader spectrum (Fig. 6), which is reflected in a higher standard deviation of  $\pm 0.23$  compared to long-term  $\pm 0.14$ , but did neither show a shift towards TD nor TA.

BGD

10, 2705–2765, 2013

## Coastal thermo-erosion in the Laptev Sea

F. Günther et al.

Title Page

Abstract

Introduction

Conclusions

References

Tables

Figures

⏪

⏩

◀

▶

Back

Close

Full Screen / Esc

Printer-friendly Version

Interactive Discussion



## 4.2 Coastal thermo-erosion at Buor Khaya

Long-term coastal erosion along the west coast of the Buor Khaya Peninsula is  $-0.55 \text{ ma}^{-1}$  ( $\pm 0.5$ ) for TD and  $-0.5 \text{ ma}^{-1}$  ( $\pm 0.4$ ) for TA. Distributions of both were skewed towards small erosion rates (Fig. 3). At site-specific greater erosion rates ( $\leq 1 \text{ ma}^{-1}$ ), as well as at very slow rates, TD is observed more often than TA. On Buor Khaya, long-term thermo-erosion was spatially highly variable along the coastline (Fig. 8). A thermokarst lagoon at  $71^\circ 47' \text{ N}$  forms the center of a weakly pronounced elongated concave coastline section where no erosional activity was observed. Our results indicate that, north of the thermokarst lagoon the coast is influenced by prevailing TA, while TD is the dominant process north and south of the Orto-Stan River mouth at  $71^\circ 34' \text{ N}$ . However, the largest contrasts in erosional patterns are not observed on a regional scale, but rather associated with variations in coastal geomorphology. Based on the geomorphological classification of transects, alas lagged behind yedoma coasts with  $-0.3 \text{ ma}^{-1}$  compared to  $-1 \text{ ma}^{-1}$  for TD, and  $0.4 \text{ ma}^{-1}$  compared to  $0.7 \text{ ma}^{-1}$  for TA. Figure 5 shows clustering of long-term TD and TA values at a low level, with some exceptions of high TD in conjunction with high TA rates, but for yedoma coasts. Coherence of TD and TA for alas coasts ( $r^2 = 0.82$ ) at Buor Khaya is lowest of the three sites, and in particular for yedoma coasts this correlation is only weak ( $r^2 = 0.39$ ). NDTI varied widely from  $-0.25$  to  $0.95$  (Fig. 6), suggesting that, in contrast to the other sites, TD has dominated over the long-term at Buor Khaya.

During the short-term period, a major shift of TD and its associated variability to more rapid erosion rates ( $-7.7 \text{ ma}^{-1} \pm 4.4$ ) was observed on Buor Khaya (Fig. 7). However TA rates were more rapid as well, but remained slower ( $-1.2 \text{ ma}^{-1} \pm 0.7$ ). Consequently, short-term NDTI is highly skewed to positive values, indicating that TD has dominated at an even higher intensity here over the past few years, compared to the long-term mean (Fig. 6).

BGD

10, 2705–2765, 2013

### Coastal thermo-erosion in the Laptev Sea

F. Günther et al.

Title Page

Abstract

Introduction

Conclusions

References

Tables

Figures

◀

▶

◀

▶

Back

Close

Full Screen / Esc

Printer-friendly Version

Interactive Discussion



### 4.3 Coastal thermo-erosion at Oyogos Yar

The entire Oyogos Yar coast has been continuously eroding at mean long-term TD and TA rates of  $-3.4 \text{ ma}^{-1}$  ( $\pm 1.1$ ) and  $-3.2 \text{ ma}^{-1}$  ( $\pm 1.1$ ), respectively. Figure 3 shows TD and TA equally centered around these mean rates with a wide distribution. At slower rates, TA is observed more frequently, while at more rapid than mean rates TD prevailed. There were a few transects at yedoma coasts east of the Kondratyeva River mouth, where rates of  $\leq -6.5 \text{ ma}^{-1}$  were observed as the most rapid long-term coastal erosion rate across all three study sites. In general, the coastal erosion pattern of Oyogos Yar could be characterized as a constant increase in eastern direction of TD and TA from the west towards the middle of the study site, and then a slight decrease towards the eastern end (Fig. 9). In contrast to the other study sites, TD values along alas coasts of Oyogos Yar were somewhat higher than those for yedoma ( $-3.4$  compared to  $-3.2 \text{ ma}^{-1}$ ), while TA ( $-3.3 \text{ ma}^{-1}$  for alas) was more rapid than long-term coastal retreat rates along yedoma coasts ( $-2.5 \text{ ma}^{-1}$ ). Figure 5 shows that TD and TA along alas coasts had a linear relationship ( $r^2 = 0.96$ ), while thermo-erosion of yedoma along Oyogos Yar takes a medium position of all three study sites, resulting in a weak coupling of TD and TA ( $r^2 = 0.49$ ). At Oyogos Yar, NDTI values are densely centered around 0, with a narrow frequency distribution (Fig. 6). This is consistent with low mean NDTI values of 0.06 and  $-0.04$ , for TD and TA-dominated coastal transects respectively. However, long-term TD outpaced TA along 80 % of all yedoma transects, which is also reflected in a clearly positive NDTI of 0.18.

In contrast, there is a negative shift in short-term NDTI relative to long-term NDTI, with values spread over a broader value domain. In the recent past, TA has dominated TD at 75 % of the short-term transects with a mean short-term NDTI at Oyogos Yar of  $-0.27$  (Fig. 6). In fact, both short-term erosion rates are more rapid with mean TD rates of  $-6.2 \text{ ma}^{-1}$  ( $\pm 2.7$ ) and  $-8.3 \text{ ma}^{-1}$  ( $\pm 2.8$ ) for TA (Fig. 7).

BGD

10, 2705–2765, 2013

## Coastal thermo-erosion in the Laptev Sea

F. Günther et al.

Title Page

Abstract

Introduction

Conclusions

References

Tables

Figures

◀

▶

◀

▶

Back

Close

Full Screen / Esc

Printer-friendly Version

Interactive Discussion



#### 4.4 Coastal thermo-erosion in the Laptev Sea region

A total of 3635 transects along 182 km of coastline (for all three sites) were analyzed and quantified on a long-term scale of 39 to 43 yr. Over a mean interval of 41.7 yr across the long-term study over all three sites, mean absolute TD was 93.3 m ( $\pm 65$ ), while mean absolute TA was 89.3 m ( $\pm 63.1$ ). This equals a mean TD rate of  $-2.2 \text{ m a}^{-1}$  ( $\pm 1.55$ ) and a mean TA rate of  $-2.1 \text{ m a}^{-1}$  ( $\pm 1.49$ ). Uncertainties were about  $\delta_r \pm 0.14 \text{ m a}^{-1}$  for TD and  $\delta_r \pm 0.12 \text{ m a}^{-1}$  for TA. Table 4 lists characteristic values of coastal thermo-erosion over time. For most transects and nearly at all intensities of coastal retreat, TD and TA were proportional to one another (Fig. 3). Slight differences in magnitude of TD and TA occurred at small and large erosion rates. The majority of outliers were due to TD rates exceeding TA. We found that mean long-term TD rates, as well as their variation, were nearly identical to TA rates for each site, when considered as a whole, although maps of thermo-erosion reveal spatially highly variable erosion along the studied coastline (Figs. 4, 8, and 9). Our long-term NDTI data show mean values of 0.12 and  $-0.13$  for coastlines tending to retreat (based on our sampling) under either prevailing TD or TA, respectively. TD exceeded TA at 55% of all transects and TA outpaced TD at 45%, suggesting a slightly thermo-denudational coastal erosion regime. Figure 6 shows the skewed distribution of negative and positive NDTI values obtained from long-term measurements. When examined over a long time scale, including all transect data from Table 4, mean NDTI for TD and TA-dominated transects was 0.05 and  $-0.08$ , respectively. Figure 5 demonstrates that TD along alas coasts was directly linked to TA, while thermo-erosion on yedoma cliffs showed greater variability, as evident from associated correlation coefficients between TA and TD of  $r^2 = 0.82$  (yedoma) and  $r^2 = 0.99$  (alas), when analyzed across all three sites.

Recent erosion rates in the Laptev Sea region are at least 1.6 times more rapid than the 42 yr long-term mean. For comparison purposes, both short-term TD and TA were determined at 824 of the 3635 coastal transects, although there are differences in this proportion between the three sites, due to data availability. Assuming that the number

BGD

10, 2705–2765, 2013

### Coastal thermo-erosion in the Laptev Sea

F. Günther et al.

Title Page

Abstract

Introduction

Conclusions

References

Tables

Figures



Back

Close

Full Screen / Esc

Printer-friendly Version

Interactive Discussion



of short-term measurements sample is sufficient for comparison to long-term values, recent TA was 2.4 times and recent TD 3.0 times more rapid than long-term means. Short-term rates of erosion, whether the top or the bottom of the cliff is used as the coastline, were more rapid ( $-5.3$  to  $-5.7 \text{ ma}^{-1}$  for short-term vs.  $-2.1$  to  $-2.2 \text{ ma}^{-1}$  for long-term) and have a greater variation ( $2.8$  to  $3.2 \text{ ma}^{-1}$  vs.  $1.5$  to  $1.6 \text{ ma}^{-1}$  for long-term), than long-term rates (Table 4). This is true for each site and for all three sites considered as a group (Fig. 7). When examined for all transects where both short and long-term observations were carried out, the coast is currently retreating under prevailing TA with NDTI  $-0.04$ . This shift is primarily due to the stronger increase of TA compared to TD (Table 4).

#### 4.5 Carbon mass fluxes

Ice Complex deposits contain a significant carbon pool (Schirrmeister et al., 2011a). Strauss et al. (2012) calculate the volumetric carbon content of Ice Complex deposits by combining measured total organic-carbon (TOC) with bulk density values. The bulk density of Ice Complex sequences varies primarily due to ground-ice content rather than TOC content (Strauss et al., 2012). Ice Complex deposits on Mamontov Klyk are generally ice-supersaturated, with 160–220 % by weight (Schirrmeister et al., 2008). Segregated gravimetric ground ice content on Buor Khaya is on average 93 % and 48 % by weight for Ice Complex and alas deposits, respectively (Strauss and Schirrmeister, 2011). According to Schirrmeister et al. (2011b), Ice Complex sediments at Oyogos Yar are ice-supersaturated with ice contents up to 200 wt%. For the results shown in Table 5, we use volumetric ice contents of 10 % for thermokarst deposits in alas basins and 50 % for Ice Complex deposits constituting yedoma hills, and site specific organic carbon contents measured on coastal outcrops, based on Strauss (2013, personal communication) and Schirrmeister et al. (2011b). Extracting the backshore elevation on the landward side of our transects, we determined mean cliff height for each study site. In combination with our long-term mean annual coastal erosion rates, we used an

**BGD**

10, 2705–2765, 2013

### Coastal thermo-erosion in the Laptev Sea

F. Günther et al.

Title Page

Abstract

Introduction

Conclusions

References

Tables

Figures

◀

▶

◀

▶

Back

Close

Full Screen / Esc

Printer-friendly Version

Interactive Discussion



2.5-D approach to determine annual eroded volumes as:

$$V[\text{m}^3] = \frac{1}{2}(\text{TD} + \text{TA}) \cdot h \cdot 50 \cdot n \quad (8)$$

where TD and TA are annual rates of cliff top and cliff bottom retreat in  $\text{m a}^{-1}$ ,  $h$  is mean cliff height in [m], 50 the coastline length covered by one coastal transect in [m], and  $n$  the number of coastal transects. Table 5 shows values used to calculate carbon flux rates that result from the erosion observed in this study.

We obtained a total annual carbon flux, based on a volume of eroded material of  $5.1 \times 10^6 \pm 0.1 \times 10^6 \text{ m}^3$ , of  $85.6 \times 10^3 \pm 0.7 \times 10^3 \text{ t}$  for a total coastline length of 182 km. 28 % of this total originates from the erosion of yedoma, and 72 % from alas coasts, although 50 % of the eroded volume derives from yedoma coasts. Higher TOC contents and lower ice volumes explain the higher carbon flux from alas coasts. The mean annual land-to-sea carbon flux therefore is  $471 \pm 32.9 \text{ t}$  per km of coastline per year. Current estimate of Laptev Sea coastline length is 7500 km (Grigoriev et al., 2006). Grigoriev (2008) estimates 25 % of the Laptev Sea coast to belong to Ice Complex deposits, including alas. Based on our observations, we found that only 74 % of the studied Ice Complex coasts are actually retreating. Assuming this fraction to be representative for the rest of the Ice Complex coast, eroding Ice Complex coasts are then 1400 km. As a result, total annual carbon flux released from eroding Ice Complex coasts is about  $0.66 \times 10^6 \pm 0.05 \text{ t}$ .

## 5 Discussion

Coastal cliffs in the Laptev Sea region are influenced by the lithology and topography of the hinterland. Their erosion rates are determined by exposure to TD and TA, and the morphological resilience of the material cropping out at the waterline. Despite the potentially strong influence of exogeneous factors such as prevailing wind direction and storminess (Solomon, 2005; Lantuit et al., 2011a) and sea-ice dynamics (Are

et al., 2008), we propose that endogeneous factors, such as ground ice distribution and backshore height (Rachold et al., 2000), also cause variations in coastal erosion.

## 5.1 Spatial variations of coastal thermo-erosion rates

One source of the heterogeneity of spatial coastal erosional patterns of our sites is the variable thermokarst relief that advancing erosion encounters (Romanovskii et al., 2000). Grouping of our transects into yedoma (hills) and alas (basins) shows different extents of permafrost degradation between sites along the coast and may help to explain this spatial heterogeneity. While yedoma segments along the Mamontov Klyk coast made up 78% of the coastline analyzed, this value was 31% at Buor Khaya, and along the Dmitry Laptev Strait mainland coast only 17%. Although this estimation does not include unstudied intervening sections, the proportions are generally of this magnitude. Generally, the possibility of variation in the relative intensities of TD and TA along alas coasts is limited by low cliff heights ( $\leq 12$  m) and low ground ice content (Fig. 5). For yedoma coasts the interdependence of TD and TA is more complicated, because environmental forcing plays a much more important role and affects TD and TA differently, due to the large ground ice contents. Although intra-site specific erosion rates varied between yedoma and alas coasts, unexpectedly this was not pronounced across our study site transect, with an increased proportion of permafrost degradation landforms from west to east, mainly because of the comparatively slow rates along the Buor Khaya coast.

Erosion rates along the Mamontov Klyk coastline from Cape Lygi to the Urasalakh River mouth are much slower than around the capes Mamontov Klyk and Terpyai Tumus. External factors like the proximity of Terpyai Tumus and Mamontov Klyk to the warm waters of the Olenyok river may account for this difference. In contrast, Lantuit et al. (2011a) find relatively slow mean coastal erosion rates of  $-0.6 \text{ ma}^{-1}$  on the Bykovsky Peninsula, which is directly exposed to the Lena River. Compared to the simple and straight outline of the other sites, the Mamontov Klyk coast features coastal promontories alternating with large half-rounded inland embayments between capes,

## Coastal thermo-erosion in the Laptev Sea

F. Günther et al.

Title Page

Abstract

Introduction

Conclusions

References

Tables

Figures



Back

Close

Full Screen / Esc

Printer-friendly Version

Interactive Discussion



that probably align with former thermokarst lagoons. TA between Cape Lygi and the Urasalakh River mouth is therefore less intensive because of the sheltered sector along a concave coastline. Rapid coastal erosion rates ( $-3.4 \text{ ma}^{-1}$ ) around Cape Mamontov Klyk formed a steep 25 m high cliff, exposing homogeneous Ice Complex deposits across the whole profile (see photograph, Fig. 2). However, near the navigation mark on Cape Mamontov Klyk, where the backshore elevation is 33 m, Ice Complex deposits are underlain by sands with low ground ice content up to 10 m a.s.l. (Schirrmeyer et al., 2008). Here, mean long-term TA is only  $-1 \text{ ma}^{-1}$  and TD  $-2 \text{ ma}^{-1}$ , suggesting that poorly stratified coastal cliffs exhibit more complex erosional patterns, where upper ice-rich parts may recede faster, forming thermo-terraces, often on geological unconformities (Are et al., 2005).

Along the whole Buor Khaya coast north of the Omoloy River mouth, large sandy beaches up to 2.5 m a.s.l. high and 50 m wide, protect the shore face from the development of thermo-erosional niches. In addition, allochthonous gravel was found on the beach which is probably transported by the Orto-Stan and Omoloy rivers. This initially fluvially supplied beach material probably gradually becomes mixed along the coast with sediment from TD on coastal cliffs and TA in the nearshore zone. Unlike the other two sites, the Buor Khaya coast is west facing and hence particularly affected by prevailing westerly winds, so that swash dominates over backwash, resulting in positive budgets of beach material. Slope debris at the cliff bottom along the entire coast illustrates the episodic character of coastal thermo-erosion on Buor Khaya, where simultaneous reworking of products from TD through TA is hampered by beach morphology. Driftwood is present along much of the beach, reflecting proximity to the Lena River, but also the role of high water events in depositing material high on the beach. Based on our field observations we agree with Are (2012), who finds that the bright color of the beach material south of the thermokarst lagoon (Fig. 8) is very dissimilar to the dark greyish sediment of the adjacent Ice Complex, while north of the thermokarst lagoon, where negative NDTI values indicate prevailing TA, beach material is similar to the outcropping Ice Complex. Furthermore, single baidzharakhs (thermokarst mounds

## Coastal thermo-erosion in the Laptev Sea

F. Günther et al.

[Title Page](#)[Abstract](#)[Introduction](#)[Conclusions](#)[References](#)[Tables](#)[Figures](#)[Back](#)[Close](#)[Full Screen / Esc](#)[Printer-friendly Version](#)[Interactive Discussion](#)

from thawing Ice Complex) have been found in the field at sea level. Probably the lower Ice Complex boundary can be found here below sea level, favoring TA through a higher subsidence potential of the shore platform when thawing occurs, with subsequential increase and maintenance of higher wave energy when it is not compensated by sediment accumulation. Günther et al. (2011) report a two times steeper shoreface profile across the northern coast section compared to another study site 50 km southwards. The prevailingly positive NDTI of the southern Buor Khaya coast might therefore also be related to different angles of shoreface inclination. Shallow coastal waters in the southern part of the Buor Khaya Gulf lower wave energy at the beach, hampering abrasional material removal from the cliff bottoms. Dividing the spatial erosional pattern on Buor Khaya into a TA-dominated north and TD-dominated south, the thermokarst lagoon exhibits a gently concave shaped inland coastline, characteristic for areas of subsidence (Romanovskii et al., 2000). For the Buor Khaya Peninsula, Are et al. (2000) report cliff top (TD) retreat rates on two yedoma cliffs of  $-1.7 \text{ ma}^{-1}$  and  $-1.9 \text{ ma}^{-1}$  over a 25 yr period (1974–1999). Our 43 yr long-term record for these particular two sites show the same values, although when examined across all eroding yedoma coasts on Buor Khaya, TD is only  $-1 \text{ ma}^{-1}$ .

Most of the Oyogos Yar coastline erodes via formation of thermo-erosional niches and block failure along ice-wedge polygons, as is typical for flat, low-lying alas coasts. According to Are et al. (2002), the morphology of coastal cliffs composed of yedoma hills largely depends on high ice contents. The yedoma hills of Oyogos Yar adjacent to the Kondratyeva River mouth simply thaw away under the influence of TD (Are et al., 2005), leaving not even baidzharakhs and resulting in large positive NDTI values (Fig. 9). Additionally, the lower Ice Complex boundary is a.s.l. and TA may be slower due to the low ground ice content in underlying layers. Kaplina (2011) report that alas deposits and the layers underlying the Ice Complex dip eastwards from Cape Svyatoi Nos. This dipping is probably responsible for gradual changes in erosion rates along the Oyogos Yar coast where the material in contact with the waterline changes. Coastlines that cut through alas depressions have a low backshore elevation and usu-

**BGD**

10, 2705–2765, 2013

## Coastal thermo-erosion in the Laptev Sea

F. Günther et al.

Title Page

Abstract

Introduction

Conclusions

References

Tables

Figures

◀

▶

◀

▶

Back

Close

Full Screen / Esc

Printer-friendly Version

Interactive Discussion



## Coastal thermo-erosion in the Laptev Sea

F. Günther et al.

Title Page

Abstract

Introduction

Conclusions

References

Tables

Figures

◀

▶

◀

▶

Back

Close

Full Screen / Esc

Printer-friendly Version

Interactive Discussion



ally have NDTI values around zero, while alas coasts retreating slowly (for example those retreating at around  $-0.5 \text{ ma}^{-1}$  on Buor Khaya) may exhibit larger negative as well as positive NDTI values. Our long-term coastal erosion rates along the Oyogos Yar coast are of comparable magnitude to those find by Pizhankova and Dobrynina (2010) on the opposite side of the Dmitry Laptev Strait. On Bolshoy Lyakhovsky Island, yedoma and alas coasts are eroding at  $-5.3 \text{ ma}^{-1}$  and  $-4.1 \text{ ma}^{-1}$ , respectively, where the lower Ice Complex boundary is at or below sea level. Erosion is slower ( $-3.4 \text{ ma}^{-1}$  and  $-3.2 \text{ ma}^{-1}$ ) where ice-poor sediments crop out at sea level. Also as a result of different vertical positions of Ice Complex deposits relative to sea level on Bolshoy Lyakhovsky, Pizhankova and Dobrynina (2010) detect only 46 % of the coastline being erosive on a long-term scale.

In addition to averaged thermo-erosion rates, coastal erosion can be quantified by area of land loss. Mars and Houseknecht (2007) use raster-based quantification; we calculated the area enclosed by vectorized historical and recent coastlines. The land area lost due to erosion is delineated by historical and recent coastlines. As a case study, we calculated land loss using our long and short-term Mamontov Klyk data. Along 55.7 km of coastline effective land-loss due to TD is  $4.44 \text{ km}^2$  over the 39.8 yr mean observation period. Mean cliff top line retreat was  $-79.7 \text{ m}$  or  $-2.0 \text{ ma}^{-1}$ . Our DSAS transect data for this coastline segment, on the other hand, show consistent mean TD values of  $-81.0 \text{ m}$  and  $-2.1 \text{ ma}^{-1}$ , respectively. Analogical similarities that lay within the uncertainties of coastal change rates were observed for short-term TD and TA. Using transects at 50 m intervals is thus sufficient method for determining coastal erosion on a long as well as short-term time scale. Based on our transect data we calculate mean annual land lost along the Mamontov Klyk coast is 2050, on Buor Khaya 550 and along the Oyogos Yar coast  $3390 \text{ m}^2 \text{ km}^{-1} \text{ a}^{-1}$ .

### 5.2 Recent coastal thermo-erosion rates

Compared to the long-term rates, coastal retreat rates over the past one to four years were more rapid, despite higher uncertainties. Short-term thermo-erosion rates across

all three sites have uncertainties of  $\pm 1.41$  and  $\pm 1.22 \text{ ma}^{-1}$  for TD and TA, respectively. More rapid recent erosion rates, particularly of short-term TA rates (Fig. 7), indicate the greater marine influence at Mamontov Klyk and Oyogos Yar. On the Buor Khaya Peninsula, recent TD rates are more rapid than long-term observations (Fig. 7) and in places of up to  $-16 \text{ ma}^{-1}$ . However, short-term measurements along the Buor Khaya coast exist only for yedoma coasts, where TD generally predominates but which do not represent the majority of the coastline. TD and TA vary differently in seasonal intensity. TA is only active during the open water season and stormy sea, while TD can proceed throughout the summer season. This disproportion of time scales causes both processes not to take place with the same intensity at one time. For instance in June, when air temperatures are positive and the mainland is already free of snow, mud flows from TD accumulate on top of snow at cliff bottom, while the adjacent sea is still covered with sea-ice, preventing TA. In late September, TD is slowed down due to re-freezing of the active layer and coastal slopes, while TA may still proceed until land fast ice develops.

In general, more rapid erosion over the past few years (mean observation period of 2.3 yr) may reflect the normal temporal variability of coastal erosion rates, or might reflect an increase in rates over the long-term mean. Examples of observed temporal variability exist: Sisko (1970) finds a four year cyclicality of thermo-abrasion intensity on the island of New Siberia. Vasiliev et al. (2011) record a 20 yr cyclicality of erosion along the western coast of the Yamal Peninsula, where the mean coastal erosion rate is  $-1.7 \text{ ma}^{-1}$  and does not experience direct climate forcing. However, remote sensing time series analysis of Jones et al. (2009) reveal a steady increase of coastal erosion intensity on the Alaska Beaufort Sea coast, with almost a doubling of rates to  $-13.6 \text{ ma}^{-1}$  recently. We observed that, short-term rates of both TD and TA are more rapid than long-term rates for all three sites at the same time, suggesting a larger spatial forcing that affects all three sites.

## Coastal thermo-erosion in the Laptev Sea

F. Günther et al.

[Title Page](#)[Abstract](#)[Introduction](#)[Conclusions](#)[References](#)[Tables](#)[Figures](#)[◀](#)[▶](#)[◀](#)[▶](#)[Back](#)[Close](#)[Full Screen / Esc](#)[Printer-friendly Version](#)[Interactive Discussion](#)

### 5.3 Normalized Difference Thermo-erosion Index (NDTI) and relevance of its components

Nearly identical long-term TD and TA rates, as well as their variations, suggest that long-term evolution of the coasts is a continuous process, where cliff bottom and cliff top line retreat are interdependent (Table 4). This is questioned by Are (2012). Shur et al. (2002) also describe the phenomenon of different behaviour of yedoma cliffs regarding relative intensities of cliff top and cliff bottom erosion. Are (2012) notices that TD along yedoma hills is usually faster than TA, and concludes that cliff top retreat does not depend on sea erosion, and that the cliff top line cannot be regarded as the primary coastline. NDTI permits us to evaluate the relative importance of TD and TA to the mechanics of arctic coastal erosion.

Along coasts with horizontally continuous ground ice layers like on the Yamal Peninsula (Streletsкая et al., 2006) and in the Canadian Arctic (Fritz et al., 2011), a decoupling of cliff top and cliff bottom retreat is observed in thermo-cirques (Kizyakov et al., 2006), and retrogressive thaw slumps (Lantuit and Pollard, 2005). On Herschel Island in NW Canada, Lantuit and Pollard (2008) observe average headwall retreat rates of  $-9.6 \text{ m a}^{-1}$  that outpace mean coastal retreat of only  $-0.6 \text{ m a}^{-1}$ . This would equal a high NDTI value of 0.88. Our NDTI data for TD along yedoma coasts is an order of magnitude lower. This suggests that TD and TA are coupled by the presence of segregated ground ice and syngenetic ice wedges in permafrost deposits, such as Ice Complex, that extend downward to the waterline. If so, NDTI serves as an indirect geomorphometrical parameter for vertical ground ice distribution along eroding permafrost coasts.

To interpret our observations of recently higher coastal erosion rates, we primarily take advantage of the NDTI concept, as a proxy for the quality of thermo-erosion. Mean short-term NDTI data was positive over the long-term and negative over the short-term observation period at Oyogos Yar, and vice versa at Buor Khaya. NDTI along the Mamontov Klyk coast was similar for the long and short term periods, in both

BGD

10, 2705–2765, 2013

## Coastal thermo-erosion in the Laptev Sea

F. Günther et al.

Title Page

Abstract

Introduction

Conclusions

References

Tables

Figures

◀

▶

◀

▶

Back

Close

Full Screen / Esc

Printer-friendly Version

Interactive Discussion



## Coastal thermo-erosion in the Laptev Sea

F. Günther et al.

Title Page

Abstract

Introduction

Conclusions

References

Tables

Figures



Back

Close

Full Screen / Esc

Printer-friendly Version

Interactive Discussion



cases reflecting the equivalence of TD and TA. From these data we hypothesize that, depending on the site characteristics of either offshore-marine (Mamontov Klyk and Oyogos Yar) or bay-marine (Buor Khaya), changing environmental conditions such as longer open water seasons and higher air temperatures, will have different impact on coastal erosion. Markus et al. (2009) observe an increase in the duration of the sea ice melt season for the Laptev/East Siberian seas of 10 days per decade for the last 30 yr, 7 days of which are due to later freezeup in fall. Boike et al. (2012) record the very warm summer of 2010 in the Lena Delta region. Both may contribute to increasing speeds of TD and TA as components of coastal thermo-erosion in the Laptev Sea region.

Mass flux rates increase most when coastal thermo-erosion increases with an NDTI close to 0 (Günther et al., 2012). Rapid TD depends on the exposure of an ice wall. The rate of mass flux in the coastal waters can increase if TD forcing changes by active layer deepening (Shiklomanov et al., 2012), higher precipitation, and air temperatures. However, as TD progresses, the cliff slope becomes more gentle, less ice is exposed and TD becomes self-limiting. TA is limited by material removal through waves, which can also limit the effectiveness of TD. In terms of changing environmental conditions forcing coastal erosion, we suggest that a longer period of open coastal waters, in particular during the autumn storm season as observed by Markus et al. (2009) and its consequently higher wave energy, could prove to be the major factor regulating whether the recently observed rapid erosion will remain at this level.

### 5.4 Impact of coastal thermo-erosion on land-to-shelf interactions and carbon fluxes

All studied coastline segments are bordered by large accumulation zones, illustrating the removal and transportation of erosion products by currents. Coastal erosion is an agent of land-shelf interactions, influencing drainage development in the coastal hinterland. The drainage network in our study sites is developed towards the coast, as described above (see Sect. 2). Progression of the coastline towards the mainland leads to rising local relief energy and subsequent compensating geomorphological processes.

## Coastal thermo-erosion in the Laptev Sea

F. Günther et al.

Title Page

Abstract

Introduction

Conclusions

References

Tables

Figures



Back

Close

Full Screen / Esc

Printer-friendly Version

Interactive Discussion



Further development of drainage systems in the coastal lowlands will result in drainage events of thermokarst lakes. Van Huissteden et al. (2011) highlight the importance of thermokarst lake drainage on permafrost ecosystems. Jones et al. (2011) dedicate attention to thermokarst lake expansion and drainage on the Seward Peninsula, Alaska.

5 They find total lake surface area is currently decreasing by 15%. In a thermokarst change detection study on Kurungnakh Island in the central Lena Delta, Günther et al. (2010) observe 45 catastrophic lake drainage events on yedoma hills, the half of which were caused by lake tapping due to Lena River bank erosion. Lakes in this area are limited in their future development by areal and stratigraphical constraints (Morgenstern et al., 2011), and consequently lake drainage was outpacing lake expansion, result-  
10 ing in a decrease of limnicity on Kurungnakh. This example illustrates the far reaching impact of coastal erosion on adjacent territories.

Grigoriev (2004) suggest that the entire coastal segment of Mamontov Klyk is one of the most active in terms of coastal erosion and that, as a result, it plays an important  
15 role in the sediment and organic carbon balance of the Laptev Sea. In fact, across our study sites, the relative proportions of yedoma and alas coastline segments are highest in favor of non-degraded yedoma at Mamontov Klyk, representing a large pool of clastic material and organic carbon by itself, and a source of these due to high coastal erosion rates.

20 Along the west coast of the Buor Khaya Peninsula we see alternating alas basins with yedoma hills. The draining effect of the sea is well-documented by recently drained thermokarst lakes in coastal proximity. Based on our RapidEye data, we estimate the limnicity of the Buor Khaya Peninsula due to large lakes is  $\approx 9\%$ , while the abundance of large thermokarst lakes along the west coast is somewhat higher with 11%. Re-  
25 cently strongly increased TD rates are likely to create pathways for lake drainage and effectively for sea expansion, depending on lake depth probably also in the form of thermokarst lagoons, enlarging the specific coastline length.

Regarding the coastal lowland at Oyogos Yar, Gavrilov et al. (2006) comment that, the draining effect of the sea in this area of neotectonic subsidence is illustrated by

the almost complete absence of thermokarst lakes within a buffer of 10 km landwards. Because of the almost flat topography and mature thermokarst relief at Oyogos Yar, we therefore do not expect higher coastal erosion rates to have greater impacts on the landscape drainage system. However, as a site of thick Ice Complex accumulation during the late Pleistocene and as a result of subsequent marine transgression in the Holocene (Romanovskii et al., 2000), the Dmitry Laptev Strait provides a large potential of continuous material resuspension (Are et al., 2008). Consequently, increased material fluxes due to higher TA rates along the Oyogos Yar coast will have great influence on water quality and turbidity in the Dmitry Laptev Strait.

We have limited our coastal erosion and carbon flux analyses only to eroding coastlines of the Ice Complex, i.e. those sections for which TOC contents and erosion rates are higher than average for the Laptev Sea and for the Arctic Ocean. Ping et al. (2011) classified the Alaska Beaufort Sea coastline into 8 geomorphic units and estimated annual organic carbon fluxes from coastal erosion of 21 to 163 kg per meter coastline. In our study a distinction was made between coastline segments that are composed of Ice Complex and alas deposits. In this way, we found annual carbon flux ranged from  $88 \pm 21.0$  to  $800 \pm 61.1$  t per km of coastline per year. To generate the magnitude of coastal erosion carbon fluxes described in other studies (e.g.  $12 \text{ Tg a}^{-1}$  for the Laptev Sea in Vonk et al., 2012) would require either more than 34 000 km of similar Ice Complex coastline, or erosion rates more than 18 times higher than the long-term rates observed here. Our study covers 10 % of the entire Ice Complex coastline of the Laptev Sea and includes a wide range of different proportions of regional Ice Complex degradation, rather than relying on a point measurement. Since we focused our study systematically on coasts with active ongoing thermo-erosion, well distributed along the mainland coast, our estimates of organic carbon fluxes from Ice Complex deposits over the entire Laptev Sea, might be considered not as conservative, although they are only a third the amount as previously stated in preliminary estimations of Grigoriev et al. (2004). However, if we had extrapolated our site-specific carbon fluxes to the Laptev Sea based only on the data from Buor Khaya, this would have resulted in

## Coastal thermo-erosion in the Laptev Sea

F. Günther et al.

[Title Page](#)[Abstract](#)[Introduction](#)[Conclusions](#)[References](#)[Tables](#)[Figures](#)[Back](#)[Close](#)[Full Screen / Esc](#)[Printer-friendly Version](#)[Interactive Discussion](#)

5 a value ten times lower than if calculated exclusively based on the Oyogos Yar data  
( $0.12 \times 10^6 \pm 0.03 \text{ t}$  compared to  $1.12 \times 10^6 \pm 0.08 \text{ t}$ ). Although our estimates of annual  
carbon flux ( $0.66 \times 10^6 \pm 0.05 \text{ t}$ ) resulting from coastal erosion in the Laptev Sea compares well with the middle of these two extremes, upscaling of TOC fluxes from coastal  
erosion should include cautious appraisal of Ice Complex coastline length, effectively  
10 eroded volumes due to the different impact of TD and TA, and the spatial and temporal heterogeneity of coastal thermo-erosion. In a study of the five largest arctic rivers, paying particular attention to the historical undersampled spring melt, Raymond et al. (2007) quantify the mean annual dissolved organic carbon flux from the Lena River as  
15  $5.83 \times 10^6 \text{ t}$ , exceeding coastal carbon fluxes in the Laptev Sea region by a multiple. However, whereas rivers transport young organic carbon, largely derived from recently fixed carbon in plant litter and upper soil horizons (Benner et al., 2004), coastal thermo-erosion mobilizes old carbon stored in permafrost, which can be considered as an additional source to present carbon cycle. In addition, riverine dissolved organic carbon  
is released over a relatively confined area to the shelf sea during the spring freshet, when water temperatures are low, whereas coastal carbon is released in late summer in a distributed fashion to the coastal waters. Changes to coastally-derived fluxes may therefore have a greater impact on ecosystem functioning.

## 6 Conclusions

20 In this study we present coastal thermo-erosion rates of three mainland sites with different degrees of permafrost degradation in the Laptev Sea region. Our long-term data are derived from change detection using remote sensing data and serve as a benchmark for intersite comparison and for comparison with modern coastal erosion rates. Across all study sites, recent erosion rates were at least 1.6 times higher than the long-term mean. Thermo-erosion rates varied along the coastline between 0 and  $-21 \text{ m a}^{-1}$ ,  
25 illustrating the high variability of coastal thermo-erosion.

### Coastal thermo-erosion in the Laptev Sea

F. Günther et al.

Title Page

Abstract

Introduction

Conclusions

References

Tables

Figures



Back

Close

Full Screen / Esc

Printer-friendly Version

Interactive Discussion



## Coastal thermo-erosion in the Laptev Sea

F. Günther et al.

Title Page

Abstract

Introduction

Conclusions

References

Tables

Figures



Back

Close

Full Screen / Esc

Printer-friendly Version

Interactive Discussion



By examining coastal retreat of the cliff top (TD) and bottom (TA) separately, we distinguish between processes responsible for thermo-erosion. TD leads to high erosion rates when near surface ice-rich layers are exposed along the cliff top line, but is not necessarily accompanied by larger eroded sediment volumes unless TA is also rapid. The Normalized Difference Thermo-erosion Index (NDTI) is a dimensionless index that qualitatively describes the relative proportions of TD and TA. Positive NDTI values indicate prevailing TD and negative NDTI that TA dominates. Despite spatially variable relative intensities of TD and TA at each study site, when considered as a set, NDTI values indicate that TD and TA are of equal importance to thermo-erosion on a regional scale. High ice contents of the yedoma coasts couple the processes since the entire coastal cliff profile is super-saturated with respect to ice, largely due to thick syngenetic ice wedges from the cliff top down to sea level. TD and TA along low-lying alas coasts are strongly coupled by topographic constraints.

The results of our planimetric coastal erosion quantification and backshore height information from DEMs were used for calculating mass fluxes in the coastal zone. We showed that thermo-erosion of coastlines composed of Pleistocene Ice Complex permafrost deposits at our study sites along the western and eastern Laptev Sea coast and the Dmitry Laptev Strait released on average  $471 \pm 32.9$  tonnes of organic-carbon per km of coastline per year. Upscaling our observations to the entire Ice Complex coastline in the Laptev Sea region, corresponds to a total annual carbon flux released from coastal erosion about  $0.66 \times 10^6 \pm 0.05$  t, which is substantially lower than some previous estimates and corresponds to one-eighth of the carbon transported by the Lena River, but is spatially and temporally more evenly distributed along the shallow Laptev Sea shelf.

The coastlines examined here are one of the most ice and carbon rich in the Arctic, and therefore particularly sensitive to climate change, while playing a potential role as a feedback to the climate cycle. If coastal erosion and the concomitant release of carbon to the shelf seas are increasing as a result of recent warming and sea ice

changes, our results suggest that these increases are only recent but represent an almost doubling of erosion rates on a decadal time scale or less.

*Acknowledgements.* We thank all Russian and German colleagues in organizing and realizing the expeditions to the Buor Khaya Peninsula and to Mamontov Klyk, in particular the pleasant collaboration in the field of I. Yakshina, A. Baranskaya, T. Opel, W. Schneider and A. Makarov. We greatly appreciate the logistical support of our partners from the Tiksi Hydrobase, the Lena Delta Reserve, and from the Arctic and Antarctic Research Institute, St. Petersburg – Russian Federation. We express our special thanks to J. Strauss, who kindly provided his calculations on organic carbon content of Ice Complex deposits. We are grateful for the technical support provided by H. Raggam and K. Gutjahr from the Institute of Digital Image Processing, Joanneum Research, Graz – Austria. S. Stettner thankfully helped with CORONA rectification for the Mamontov Klyk study site. RapidEye imagery have been gratefully provided by the German Aerospace Center through the RapidEye Science Archive. ALOS PRISM and KOMPSAT-2 data were kindly provided by JAXA and ESA through the International Polar Year – Arctic Circumpolar Coastal Observatory Network (project ID 4133) and the LEDAM project (awarded by ESA ADEN, ID 3616). SPOT-5 imagery were kindly provided by SPOT Planet Action – an Austrian GEO initiative (project: Coastal erosion in East Siberia). S. Wetterich and L. Schirrmeister thankfully helped to enhance the manuscript with careful content revisions and constructive comments. We acknowledge the support of German Ministry of Science and Education funding this research through the Potsdam Research Cluster for Georisk Analysis, Environmental Change and Sustainability (PROGRESS). This work was also made possible by support from the Helmholtz Association's through a Joint Russian-German Research Group (HGF-JRG 100).

## References

- AMAP: Snow, Water, Ice and Permafrost in the Arctic (SWIPA): Climate Change and the Cryosphere, Arctic Monitoring and Assessment Programme (AMAP), Oslo, Norway, available at: [www.amap.no](http://www.amap.no), 2011. 2707
- Are, F. E.: Thermal abrasion of sea coasts, *Polar Geography and Geology*, 12, 87–157, doi:10.1080/10889378809377352, from: *Termoabraziya morskikh beregov*, Moscow, Nauka, 1980, 158 pp., 1988a. 2708, 2709

## Coastal thermo-erosion in the Laptev Sea

F. Günther et al.

Title Page

Abstract

Introduction

Conclusions

References

Tables

Figures



Back

Close

Full Screen / Esc

Printer-friendly Version

Interactive Discussion



- Are, F. E.: Thermal abrasion of sea coasts, *Polar Geography and Geology*, 12, 87–157, from: *Termoabraziya morskikh beregov*, Moscow, Nauka, 1980, 158 pp., 1988b. 2708
- Are, F. E.: The role of coastal retreat for sedimentation in the Laptev Sea, in: *Land-Ocean Systems in the Siberian Arctic*, edited by Kassens, H., Bauch, H. A., Dmitrenko, I. A., Eicken, H., Hubberten, H.-W., Melles, M., Thiede, J., and Timokohov, L. A., 287–295, Springer, 1999. 2708
- Are, F. E.: Razrushenie beregov arkticheskikh primorskikh nizmennostej (Coastal erosion of the Arctic lowlands), Academic publishing house “Geo”, Novosibirsk, 2012. 2729, 2733
- Are, F. E., Grigoriev, M. N., Hubberten, H.-W., Rachold, V., Razumov, S. O., and Schneider, W.: Coastal erosion studies in the Laptev Sea, in: *Russian-German Cooperation System Laptev Sea: The Expedition Lena 1999*, edited by: Rachold, V., vol. 354, Reports on Polar and Marine Research, Alfred Wegener Institute, available at: <http://epic.awi.de/26534/>, chap. 4.3, 65–74, 2000. 2730
- Are, F., Grigoriev, M. N., Hubberten, H.-W., Rachold, V., Razumov, S. O., and Schneider, W.: Comparative shoreface evolution along the Laptev Sea coast, *Polarforschung*, 70, 135–150, 2002. 2713, 2730
- Are, F. E., Grigoriev, M. N., Hubberten, H.-W., and Rachold, V.: Using thermoterrace dimensions to calculate the coastal erosion rate, *Geo-Mar. Lett.*, 25, 121–126, doi:10.1007/s00367-004-0193-y, 2005. 2709, 2729, 2730
- Are, F. E., Reimnitz, E., Grigoriev, M. N., Hubberten, H.-W., and Rachold, V.: The influence of cryogenic processes on the erosional arctic shoreface, *J. Coast. Res.*, 24, 110–121, doi:10.2112/05-0573.1, 2008. 2727, 2736
- Asplin, M. G., Galley, R., Barber, D. G., and Prinsenber, S.: Fracture of summer perennial sea ice by ocean swell as a result of Arctic storms, *J. Geophys. Res.*, 117, C06025, doi:10.1029/2011JC007221, 2012. 2707
- Benner, R., Benitez-Nelson, B., Kaiser, K., and Amon, R. M. W.: Export of young terrigenous dissolved organic carbon from rivers to the Arctic Ocean, *Geophys. Res. Lett.*, 31, L05305, doi:10.1029/2003GL019251, 2004. 2707, 2737
- Boike, J., Kattenstroth, B., Abramova, K., Bornemann, N., Chetverova, A., Fedorova, I., Fröb, K., Grigoriev, M., Grüber, M., Kutzbach, L., Langer, M., Minke, M., Muster, S., Piel, K., Pfeiffer, E.-M., Stoof, G., Westermann, S., Wischnewski, K., Wille, C., and Hubberten, H.-W.: Baseline characteristics of climate, permafrost, and land cover from a new permafrost observatory

---

## Coastal thermo-erosion in the Laptev Sea

F. Günther et al.

---

[Title Page](#)[Abstract](#)[Introduction](#)[Conclusions](#)[References](#)[Tables](#)[Figures](#)[Back](#)[Close](#)[Full Screen / Esc](#)[Printer-friendly Version](#)[Interactive Discussion](#)

## Coastal thermo-erosion in the Laptev Sea

F. Günther et al.

Title Page

Abstract

Introduction

Conclusions

References

Tables

Figures

◀

▶

◀

▶

Back

Close

Full Screen / Esc

Printer-friendly Version

Interactive Discussion



in the Lena River Delta, Siberia (1998–2011), *Biogeosciences Discuss.*, 9, 13627–13684, doi:10.5194/bgd-9-13627-2012, 2012. 2734

Charkin, A. N., Dudarev, O. V., Semiletov, I. P., Kruhmalev, A. V., Vonk, J. E., Sánchez-García, L., Karlsson, E., and Gustafsson, Ö.: Seasonal and interannual variability of sedimentation and organic matter distribution in the Buor-Khaya Gulf: the primary recipient of input from Lena River and coastal erosion in the southeast Laptev Sea, *Biogeosciences*, 8, 2581–2594, doi:10.5194/bg-8-2581-2011, 2011. 2707

Comiso, J. C., Parkinson, C. L., Gersten, R., and Stock, L.: Accelerated decline in the Arctic sea ice cover, *Geophys. Res. Lett.*, 35, L01703, doi:10.1029/2007GL031972, 2008. 2707

Dmitrenko, I. A., Kirillov, S. A., Tremblay, L. B., Kassens, H., Anisimov, O. A., Lavrov, S. A., Razumov, S. O., and Grigoriev, M. N.: Recent changes in shelf hydrography in the Siberian Arctic: potential for subsea permafrost instability, *J. Geophys. Res.*, 116, C10027, doi:10.1029/2011JC007218, 2011. 2707

Drachev, S. S., Savostin, L. A., Groshev, V. G., and Bruni, I. E.: Structure and geology of the continental shelf of the Laptev Sea, Eastern Russian Arctic, *Tectonophysics*, 298, 357–393, doi:10.1016/S0040-1951(98)00159-0, 1998. 2711

Dunaev, N. N. and Nikiforov, S. L.: Shelf i berega arkticheskikh morei (Shelf and coasts of arctic seas), in: *Geoekologiya shelfa i beregov morei Rossii (Geoecology of shelf and coasts of Russian seas)*, edited by: Aibulatov, N. A., Noosphera, Moscow, chap. 2, 27–242, 2001. 2711, 2713

Dupeyrat, L., Costard, F., Randriamazaoro, R., Gailhardis, E., Gautier, E., and Fedorov, A.: Effects of ice content on the thermal erosion of permafrost: implications for coastal and fluvial erosion, *Permafrost Periglac.*, 22, 179–187, doi:10.1002/ppp.722, 2011. 2708

Ehlers, M., Klonus, S., Åstrand, P. J., and Rosso, P.: Multi-sensor image fusion for pansharpening in remote sensing, *International J. Image Data Fus.*, 1, 25–45, doi:10.1080/19479830903561985, 2010. 2717

Forbes, D. L. (Ed.): *State of the Arctic Coast 2010 – Scientific Review and Outlook*, International Arctic Science Committee, Land-Ocean Interactions in the Coastal Zone, Arctic Monitoring and Assessment Programme, International Permafrost Association, Helmholtz-Zentrum, Geesthacht, Germany, available at: <http://arcticcoasts.org>, 2011. 2707

Fraser, C. S. and Ravanbakhsh, M.: Georeferencing accuracy of GeoEye-1 imagery, *Photogramm. Eng. Rem. S.*, 75, 634–638, 2009. 2715

## Coastal thermo-erosion in the Laptev Sea

F. Günther et al.

Title Page

Abstract

Introduction

Conclusions

References

Tables

Figures



Back

Close

Full Screen / Esc

Printer-friendly Version

Interactive Discussion



- Fritz, M., Wetterich, S., Meyer, H., Schirrmeyer, L., Lantuit, H., and Pollard, W. H.: Origin and characteristics of massive ground ice on Herschel Island (western Canadian Arctic) as revealed by stable water isotope and hydrochemical signatures, *Permafrost Periglac.*, 22, 26–38, doi:10.1002/ppp.714, 2011. 2733
- 5 Gavrilov, A. V., Romanovskii, N. N., Romanovsky, V. E., Hubberten, H.-W., and Tumskoy, V. E.: Reconstruction of ice complex remnants on the eastern Siberian arctic shelf, *Permafrost Periglac.*, 14, 187–198, doi:10.1002/ppp.450, 2003. 2718
- Gavrilov, A. V., Romanovskii, N. N., and Hubberten, H.-W.: Paleogeograficheskii scenarij poslelednikovoi transgressii na shelfe Morya Laptevykh (Paleogeographic scenario of the postglacial transgression on the Laptev Sea shelf), *Kriosfera Zemli (Earth's Cryosphere)*, 10, 39–50, 2006. 2735
- 10 Grigoriev, M. N.: Periglacial studies around Cape Mamontov Klyk – Studies of coastal dynamics and subsea permafrost, in: Russian–German Cooperation System Laptev Sea: The Expedition Lena–Anabar 2003, edited by: Schirrmeyer, L., vol. 489, Reports on Polar and Marine Research, Alfred Wegener Institute, available at: <http://epic.awi.de/26668/>, chap. 4.7, 139–150, 2004. 2735
- 15 Grigoriev, M. N.: Kriomorphogenez i litodinamika pribrezhno-shelfovoi zony morei Vostochnoi Sibiri (Cryomorphogenesis and lithodynamics of the East Siberian near-shore shelf zone), Habilitation thesis, SB RAS Permafrost Institute, Yakutsk, 2008. 2709, 2710, 2718, 2727
- 20 Grigoriev, M. N., Are, F. E., Hubberten, H.-W., Rachold, V., Razumov, S. O., and Schneider, W.: Onshore coastal studies – coastal dynamics at key sites of the New Siberian Islands, Dmitry Laptev Strait, and Buor Khaya Bay, in: Russian–German Cooperation System Laptev Sea: The Expedition Lena 2002, edited by: Grigoriev, M. N., Rachold, V., Bolshiyarov, D. Y., Pfeiffer, E.-M., Schirrmeyer, L., Wagner, D., and Hubberten, H.-W., vol. 466, Reports on Polar and Marine Research, Alfred Wegener Institute, available at: <http://epic.awi.de/26645/>, chap. 5.3.3, 326–329, 2003. 2709
- 25 Grigoriev, M. N., Rachold, V., Schirrmeyer, L., and Hubberten, H.-W.: Organic carbon input to the Arctic Seas through coastal erosion, in: *The Organic Carbon Cycle in the Arctic Ocean: Present and Past*, edited by: Stein, R. and Macdonald, R. W., Springer, Berlin, chap. 2.3, 37–65, 2004. 2708, 2736
- 30 Grigoriev, M. N., Razumov, S. O., Kunitzky, V. V., and Spektor, V. B.: Dinamika beregov vostochnykh arkticheskikh morey Rossii: Osnovnye faktory, zakonomernosti i tendencii (Dy-

## Coastal thermo-erosion in the Laptev Sea

F. Günther et al.

Title Page

Abstract

Introduction

Conclusions

References

Tables

Figures

◀

▶

◀

▶

Back

Close

Full Screen / Esc

Printer-friendly Version

Interactive Discussion



namics of the Russian East Arctic Sea coast: major factors, regularities and tendencies), *Kriosfera Zemli (Earth's Cryosphere)*, 10, 74–94, 2006. 2708, 2727

Grigoriev, M. N., Kunitsky, V. V., Chzhan, R. V., and Shepelev, V. V.: On the variation in geocryological, landscape and hydrological conditions in the Arctic zone of East Siberia in connection with climate warming, *Geogr. Natur. Resour.*, 30, 101–106, doi:10.1016/j.gnr.2009.06.002, 2009. 2710

Grosse, G., Schirrmeister, L., Kunitsky, V. V., and Hubberten, H.-W.: The use of CORONA images in remote sensing of periglacial geomorphology: an illustration from the NE Siberian coast, *Permafrost Periglac.*, 16, 163–172, doi:10.1002/ppp.509, 2005. 2716

Grosse, G., Schirrmeister, L., and Malthus, T. J.: Application of Landsat-7 satellite data and a DEM for the quantification of thermokarst-affected terrain types in the periglacial Lena–Anabar coastal lowland, *Polar Res.*, 25, 51–67, doi:10.1111/j.1751-8369.2006.tb00150.x, 2006. 2712, 2752

Grosse, G., Romanovsky, V., Jorgenson, T., Walter Anthony, K. M., Brown, J., and Overduin, P. P.: Vulnerability and feedbacks of permafrost to climate change, *Eos Trans. AGU*, 92, 73–74, doi:10.1029/2011EO090001, 2011. 2708

Günther, F., Ulrich, M., Morgenstern, A., and Schirrmeister, L.: Planimetric and volumetric thermokarst change detection on ice rich permafrost, using remote sensing and field data, in: Abstracts from the Third European Conference on Permafrost: Thermal State of Frozen Ground in a Changing Climate During the IPY, Svalbard, Norway, 13–17 June 2010, edited by: Mertes, J. R., Christiansen, H. H., and Etzelmüller, B., The University Centre in Svalbard, available at: <http://epic.awi.de/22795/>, 2010. 2735

Günther, F., Overduin, P. P., and Sandakov, A. V.: Topographical surveys for coastal dynamics studies, in: Russian–German Cooperation System Laptev Sea: The Expedition Eastern Laptev Sea – Buor Khaya Peninsula 2010, edited by: Wetterich, S., Overduin, P. P., and Grigoriev, M. N., vol. 629, Reports on Polar and Marine Research, Alfred-Wegener-Institute, chap. 4, 17–34, 2011. 2717, 2730

Günther, F., Overduin, P. P., Sandakov, A. V., Grosse, G., and Grigoriev, M. N.: Thermo-erosion along the Yedomo Coast of the Buor Khaya Peninsula, Laptev Sea, East Siberia, in: Proceedings of the Tenth International Conference on Permafrost, Salekhard, Yamal-Nenets Autonomous District, Russia, June 25–29, edited by: Hinkel, K. M., vol. 1, International Contributions, 137–142, 2012. 2710, 2721, 2734

## Coastal thermo-erosion in the Laptev Sea

F. Günther et al.

Title Page

Abstract

Introduction

Conclusions

References

Tables

Figures

◀

▶

◀

▶

Back

Close

Full Screen / Esc

Printer-friendly Version

Interactive Discussion



- Imaeva, L. P., Kozmin, B. M., Sergeyenko, A. I., Belolyubskii, I. N., and Siegert, C.: Noveyshie struktury, stratigrafiya kvartera i sovremennaya geodinamika territorii arkticheskogo sektora probrezhno-shelfovoi zony Severnogo Verkhoyana (Severo-vostok Yakutii) – (Modern structures, quaternary stratigraphy and recent geodynamics in the arctic sector of the Northern Verkhoyan coastal shelf zone (North of East Yakutia)), Bulletin of the comission on studies of the quaternary period, 67, 6–19, 2007. 2712
- Jones, B. M., Arp, C. D., Jorgenson, M. T., Hinkel, K. M., Schmutz, J. A., and Flint, P. L.: Increase in the rate and uniformity of coastline erosion in Arctic Alaska, Geophys. Res. Lett., 36, L03503, doi:10.1029/2008GL036205, 2009. 2707, 2718, 2732
- Jones, B. M., Grosse, G., Arp, C. D., Jones, M. C., Walter Anthony, K. M., and Romanovsky, V. E.: Modern thermokarst lake dynamics in the continuous permafrost zone, northern Seward Peninsula, Alaska, J. Geophys. Res., 116, G00M03, doi:10.1029/2011JG001666, 2011. 2718, 2735
- Kamiya, I.: Reduction of JPEG Noise from the ALOS PRISM Products, Bulletin of the Geographical Survey Institute, 55, 31–38, 2008. 2717
- Kaplina, T. N.: Nekotorye osobennosti razmyva beregov, slozhennykh mnogoletnemerzlymi gornymi porodami (Some features of coastal thermoerosion of frozen bluffs), Questions of sea coast research, Publishing House of the USSR Academy of Sciences, Moscow, 113–117, 1959. 2709
- Kaplina, T. N.: Drevnie alasnye komplekсы Severnoi Yakutii – soobshchenie 2 (Ancient alas complexes of Northern Yakutia – part 2), Kriosfera Zemli (Earth's Cryosphere), 15, 20–30, 2011. 2730
- Kholodov, A., Gilichinsky, D., Ostroumov, V., Sorokovikov, V., Abramov, A., Davydov, S., and Romanovsky, V.: Regional and local variability of modern natural changes in permafrost temperature in the Yakutian coastal lowlands, Northeastern Siberia, in: Proceedings of the Tenth International Conference on Permafrost, Salekhard, Yamal-Nenets Autonomous District, Russia, 25–29 June, edited by: Hinkel, K., vol. 1, International Contributions, 203–207, 2012. 2711
- Kizyakov, A. I., Leibman, M. O., and Perednya, D. D.: Destruktivnye rel'efobrazuyushie processy poberezhii arkticheskikh ravnin s plastovymi podzemnymi l'dami (Destructive relief-forming processes at the coasts of the arctic plains with tabular ground ice), Kriosfera Zemli (Earth's Cryosphere), 10, 79–89, 2006. 2733

## Coastal thermo-erosion in the Laptev Sea

F. Günther et al.

Title Page

Abstract

Introduction

Conclusions

References

Tables

Figures

◀

▶

◀

▶

Back

Close

Full Screen / Esc

Printer-friendly Version

Interactive Discussion



Klyuev, Y. V.: Termicheskaya abraziya pribrezhnoi polosy polyarnykh morey (Thermal erosion of the coastal zone of polar seas), *Izvestiya vsesoyuznogo geograficheskogo obshchestva* (Transactions of the all-union geographical society), 102, 129–135, 1970. 2709, 2712

Lantuit, H. and Pollard, W. H.: Temporal stereophotogrammetric analysis of retrogressive thaw slumps on Herschel Island, Yukon Territory, *Nat. Hazards Earth Syst. Sci.*, 5, 413–423, doi:10.5194/nhess-5-413-2005, 2005. 2733

Lantuit, H. and Pollard, W. H.: Fifty years of coastal erosion and retrogressive thaw slump activity on Herschel Island, southern Beaufort Sea, Yukon Territory, Canada, *Geomorphology*, 95, 84–102, doi:10.1016/j.geomorph.2006.07.040, 2008. 2733

Lantuit, H., Rachold, V., Pollard, W. H., Steenhuisen, F., Ødegaard, R. S., and Hubberten, H.-W.: Towards a calculation of organic carbon release from erosion of Arctic coasts using non-fractal coastline datasets, *Mar. Geol.*, 257, 1–10, doi:10.1016/j.margeo.2008.10.004, 2009. 2718

Lantuit, H., Atkinson, D., Overduin, P. P., Grigoriev, M. N., Rachold, V., Grosse, G., and Hubberten, H.-W.: Coastal erosion dynamics on the permafrost-dominated Bykovsky Peninsula, north Siberia, 1951–2006, *Polar Res.*, 30, 7341, doi:10.3402/polar.v30i0.7341, 2011a. 2709, 2727, 2728

Lantuit, H., Overduin, P. P., Couture, N., Wetterich, S., Are, F., Atkinson, D., Brown, J., Cherkashov, G., Drozdov, D., Forbes, D. L., Graves-Gaylord, A., Grigoriev, M. N., Hubberten, H.-W., Jordan, J., Jorgenson, T., Ødegaard, R. S., Ogorodov, S., Pollard, W. H., Rachold, V., Sedenko, S., Solomon, S., Steenhuisen, F., Streletskaia, I., and Vasiliev, A.: The Arctic coastal dynamics database: a new classification scheme and statistics on arctic permafrost coastlines, *Estuar. Coast.*, 35, 383–400, doi:10.1007/s12237-010-9362-6, 2011b. 2707, 2709

Le Moigne, J., Cole-Rhodes, A. A., Eastman, R. D., Netanyahu, N. S., Stone, H. S., Zavorin, I., and Morissette, J. T.: Multitemporal and multisensor image registration, in: *Image Registration for Remote Sensing*, edited by: Le Moigne, J., Netanyahu, N. S., and Eastman, R. D., Cambridge University press, chap. 14, 293–338, 2011. 2715

Markus, T., Stroeve, J. C., and Miller, J.: Recent changes in Arctic sea ice melt onset, freezeup, and melt season length, *J. Geophys. Res.-Oceans*, 114, C12024, doi:10.1029/2009JC005436, 2009. 2734

## Coastal thermo-erosion in the Laptev Sea

F. Günther et al.

Title Page

Abstract

Introduction

Conclusions

References

Tables

Figures



Back

Close

Full Screen / Esc

Printer-friendly Version

Interactive Discussion



- Mars, J. C. and Houseknecht, D. W.: Quantitative remote sensing study indicates doubling of coastal erosion rate in past 50 yr along a segment of the Arctic coast of Alaska, *Geology*, 35, 583–586, doi:10.1130/G23672A.1, 2007. 2731
- Maslanik, J., Stroeve, J., Fowler, C., and Emery, W.: Distribution and trends in Arctic sea ice age through spring 2011, *Geophys. Res. Lett.*, 38, L13502, doi:10.1029/2011GL047735, 2011. 2707
- Morgenstern, A., Grosse, G., Günther, F., Fedorova, I., and Schirrmeyer, L.: Spatial analyses of thermokarst lakes and basins in Yedoma landscapes of the Lena Delta, *The Cryosphere*, 5, 849–867, doi:10.5194/tc-5-849-2011, 2011. 2735
- Opel, T., Dereviagin, A. Y., Meyer, H., Schirrmeyer, L., and Wetterich, S.: Palaeoclimatic information from stable water isotopes of Holocene ice wedges on the Dmitrii Laptev Strait, Northeast Siberia, Russia, *Permafrost Periglac.*, 22, 84–100, doi:10.1002/ppp.667, 2011. 2713
- Overduin, P. P., Hubberten, H.-W., Rachold, V., Romanovskii, N. N., Grigoriev, M. N., and Kasymkaya, M.: The evolution and degradation of coastal and offshore permafrost in the Laptev and East Siberian Seas during the last climatic cycle, in: *Coastline Changes: Interrelation of Climate and Geological Processes*, edited by: Harff, J., Hay, W., and Tetzlaff, D., The Geological Society of America Special Paper, 426, 97–111, doi:10.1130/2007.2426(07), 2007. 2709
- Overeem, I., Anderson, R. S., Wobus, C. W., Clow, G. D., Urban, F. E., and Matell, N.: Sea ice loss enhances wave action at the Arctic coast, *Geophys. Res. Lett.*, 38, L17503, doi:10.1029/2011GL048681, 2011. 2707
- Peterson, B. J., Holmes, R. M., McClelland, J. W., Vorosmarty, C. J., Lammers, R. B., Shiklomanov, A. I., Shiklomanov, I. A., and Rahmstorf, S.: Increasing river discharge to the Arctic Ocean, *Science*, 298, 2171–2173, doi:10.1126/science.1077445, 2002. 2707
- Pieczonka, T., Bolch, T., and Buchroithner, M.: Generation and evaluation of multitemporal digital terrain models of the Mt. Everest area from different optical sensors, *Int. Soc. Photogramme.*, 66, 927–940, doi:10.1016/j.isprs.2011.07.003, 2011. 2716
- Ping, C.-L., Michaelson, G. J., Guo, L., Jorgenson, M. T., Kanevskiy, M., Shur, Y., Dou, F., and Liang, J.: Soil carbon and material fluxes across the eroding Alaska Beaufort Sea coastline, *J. Geophys. Res.*, 116, G02004, doi:10.1029/2010JG001588, 2011. 2736

## Coastal thermo-erosion in the Laptev Sea

F. Günther et al.

[Title Page](#)

[Abstract](#)

[Introduction](#)

[Conclusions](#)

[References](#)

[Tables](#)

[Figures](#)

⏪

⏩

◀

▶

[Back](#)

[Close](#)

[Full Screen / Esc](#)

[Printer-friendly Version](#)

[Interactive Discussion](#)



Pipko, I. I., Semiletov, I. P., Pugach, S. P., Wählström, I., and Anderson, L. G.: Interannual variability of air-sea CO<sub>2</sub> fluxes and carbon system in the East Siberian Sea, *Biogeosciences*, 8, 1987–2007, doi:10.5194/bg-8-1987-2011, 2011. 2708

Pizhankova, E. I. and Dobrynina, M. S.: Dinamika poberezh'ya Lyakhovskikh Ostrovov – Rezultaty deshifirovaniya aerokosmicheskikh snimkov (The dynamics of the Lyakhovsky Islands coastline – results of aerospace image interpretation), *Kriosfera Zemli (Earth's Cryosphere)*, 14, 66–79, 2010. 2709, 2718, 2731

Popov, A. I. (Ed.): *Regionalnaya Kriolitologiya (Regional Cryolithology)*, Moscow State University Publishing House, 1989. 2711

Rachold, V., Grigoriev, M. N., Are, F. E., Solomon, S., Reimnitz, E., Kassens, H., and Antonow, M.: Coastal erosion vs riverine sediment discharge in the Arctic Shelf seas, *Int. J. Earth Sci.*, 89, 450–460, doi:10.1007/s005310000113, 2000. 2708, 2728

Rachold, V., Are, F. E., Atkinson, D. E., Cherkashov, G., and Solomon, S. M.: Arctic Coastal Dynamics (ACD): an introduction, *Geo-Mar. Lett.*, 25, 63–68, doi:10.1007/s00367-004-0187-9, 2003. 2709

Raymond, P. A., McClelland, J. W., Holmes, R. M., Zhulidov, A. V., Mull, K., Peterson, B. J., Striegl, R. G., Aiken, G. R., and Gurtovaya, T. Y.: Flux and age of dissolved organic carbon exported to the Arctic Ocean: A carbon isotopic study of the five largest arctic rivers, *Global Biogeochem. Cy.*, 21, GB4011, doi:10.1029/2007GB002934, 2007. 2737

Razumov, S. O.: Permafrost as a factor of the dynamics of the coastal zone of the Russian East Arctic Seas, *Oceanology*, 50, 262–267, doi:10.1134/S0001437010020116, 2010. 2709

Razumov, S. O. and Grigoriev, M. N.: Coastal erosion as a destabilizing factor of carbonate balance in the East Siberian Arctic seas, *Kriosfera Zemli (Earth's Cryosphere)*, 15, 65–68, 2011. 2708

Romanovskii, N. N. and Tumskey, V. E.: Retrospektivnyi podkhod k ocenke sovremennogo rasprostraneniya i stroeniya shelfovoi kriolitozony Vostochnoi Arktiki (Retrospective approach to the estimation of the contemporary extension and structure of the shelf cryolithozone in East Arctic), *Kriosfera Zemli (Earth's Cryosphere)*, 15, 3–14, 2011. 2711

Romanovskii, N., Hubberten, H.-W., Gavrillov, A., Tumskey, V., Tipenko, G., Grigoriev, M., and Siegert, C.: Thermokarst and land-ocean interactions, Laptev Sea Region, Russia, *Permafrost Periglac.*, 11, 137–152, 2000. 2728, 2730, 2736

Romanovsky, V. E., Drozdov, D. S., Oberman, N. G., Malkova, G. V., Kholodov, A. L., Marchenko, S. S., Moskalenko, N. G., Sergeev, D. O., Ukraintseva, N. G., Abramov, A. A.,

## Coastal thermo-erosion in the Laptev Sea

F. Günther et al.

Title Page

Abstract

Introduction

Conclusions

References

Tables

Figures



Back

Close

Full Screen / Esc

Printer-friendly Version

Interactive Discussion



- Gilichinsky, D. A., and Vasiliev, A. A.: Thermal state of permafrost in Russia, *Permafrost Periglac.*, 21, 136–155, doi:10.1002/ppp.683, 2010. 2707, 2711
- ROSHYDROMET and ArcticRIMS: Lena at Kusur, stream discharge station data, available at: <http://rims.unh.edu/data/station/station.cgi?station=6342>, 2009. 2711
- 5 RSG: Remote Sensing Software Graz, software documentation, release 7.03, Institute for Digital Image Processing of Joanneum Research, Graz, Austria, 2011. 2716
- Santoro, M. and Strozzi, T.: Circumpolar digital elevation models > 55° N with links to geotiff images, eSA DUE Permafrost, DEM from Russian Topographic Maps, doi:10.1594/PANGAEA.779748, 2012. 2754
- 10 Schirrmester, L., Grosse, G., Kunitsky, V., Magens, D., Meyer, H., Dereviagin, A., Kuznetsova, T., Andreev, A., Babiy, O., Kienast, F., Grigoriev, M., Overduin, P. P., and Preusser, F.: Periglacial landscape evolution and environmental changes of Arctic lowland areas for the last 60 000 years (western Laptev Sea coast, Cape Mamontov Klyk), *Polar Res.*, 27, 249–272, doi:10.1111/j.1751-8369.2008.00067.x, 2008. 2712, 2726, 2729
- 15 Schirrmester, L., Grosse, G., Wetterich, S., Overduin, P. P., Strauss, J., Schuur, E. A. G., and Hubberten, H.-W.: Fossil organic matter characteristics in permafrost deposits of the north-east Siberian Arctic, *J. Geophys. Res.*, 116, G00M02, doi:10.1029/2011JG001647, 2011a. 2708, 2726
- Schirrmester, L., Kunitsky, V., Grosse, G., Wetterich, S., Meyer, H., Schwamborn, G., Babiy, O., Derevyagin, A., and Siegert, C.: Sedimentary characteristics and origin of the Late Pleistocene Ice Complex on north-east Siberian Arctic coastal lowlands and islands – a review, *Quaternary Int.*, 241, 3–25, doi:10.1016/j.quaint.2010.04.004, 2011b. 2708, 2713, 2726, 2756
- 20 Sekretov, S. B.: Eurasian Basin – Laptev Sea geodynamic system: tectonic and structural evolution, *Polarforschung*, 69, 51–54, 2001. 2711
- Semiletov, I. P., Pipko, I. I., Shakhova, N. E., Dudarev, O. V., Pugach, S. P., Charkin, A. N., McRoy, C. P., Kosmach, D., and Gustafsson, Ö.: Carbon transport by the Lena River from its headwaters to the Arctic Ocean, with emphasis on fluvial input of terrestrial particulate organic carbon vs. carbon transport by coastal erosion, *Biogeosciences*, 8, 2407–2426, doi:10.5194/bg-8-2407-2011, 2011. 2708
- 30 Shiklomanov, N. I., Streletskiy, D. A., and Nelson, F. E.: Northern Hemisphere component of the Global Circumpolar Active Layer Monitoring (CALM) Program, in: Proceedings of the Tenth International Conference on Permafrost, Salekhard, Yamal-Nenets Autonomous Dis-

## Coastal thermo-erosion in the Laptev Sea

F. Günther et al.

Title Page

Abstract

Introduction

Conclusions

References

Tables

Figures

◀

▶

◀

▶

Back

Close

Full Screen / Esc

Printer-friendly Version

Interactive Discussion



tract, Russia, 25–29 June 2012, edited by: Hinkel, K. M., vol. 1, International Contributions, 377–382, The Northern Publisher, Salekhard, 2012. 2734

Shur, Y., Vasiliev, A., Kanevskiy, M., Maximov, V., Pokrovsky, S., and Zaikanov, V.: Shore Erosion in Russian Arctic, in: Cold regions Engineering – Cold Regions Impacts on Transportation and Infrastructure, edited by: Merrill, K., American Society of Civil Engineers, 736–747, 2002. 2733

Sisko, R. K.: Termoabrazionnye berega arkticheskikh morei – na primere o. Novaya Sibir (Thermo-abrasional coasts of arctic seas – on the example of the island of New Siberia), Glaciologicheskie issledovaniya v polyarnykh stranakh (glaciological research in polar regions), AANII, Leningrad, 294, 183–194, 1970. 2732

Sohn, H. G., Kim, G.-H., and Yom, J.-H.: Mathematical modelling of historical reconnaissance CORONA KH-4B imagery, Photogramm Rec, 19, 51–66, doi:10.1046/j.0031-868X.2003.00257.x, 2004. 2716

Solomon, S. M.: Spatial and temporal variability of shoreline changes in the Beaufort–Mackenzie region, northwest territories, Canada, Geo-Mar. Lett., 25, 125–137, doi:10.1007/s00367-004-0194-x, 2005. 2727

Sovershaev, V. A.: Beregovaya zona arkticheskikh morey (Coastal zone of Arctic Seas), in: Geoekologiya Severa (Geoecology of the North), edited by: Solomatina, V. I., Moscow State University Publishing House, Moscow, chap. 2.5, 55–59, 1992. 2721

Strauss, J. and Schirrmeister, L.: Permafrost sequences of Buor Khaya Peninsula, in: Russian–German Cooperation System Laptev Sea: The Expedition Eastern Laptev Sea – Buor Khaya Peninsula 2010, edited by: Wetterich, S., Overduin, P. P., and Grigoriev, M. N., vol. 629, Reports on Polar and Marine Research, Alfred-Wegener-Institute, chap. 5, 35–50, 2011. 2712, 2726

Strauss, J., Schirrmeister, L., Wetterich, S., Borchers, A., and Davydov, S. P.: Grain-size properties and organic-carbon stock of Yedoma Ice Complex permafrost from the Kolyma lowland, northeastern Siberia, Global Biogeochem. Cy., 26, GB3003, doi:10.1029/2011GB004104, 2012. 2708, 2726, 2756

Streletskaaya, I. D., Kanevskiy, M. Z., and Vasiliev, A. A.: Massive ground ice in dislocated quaternary sediments of Western Yamal, Kriosfera Zemli (Earth's Cryosphere), 10, 68–78, 2006. 2733

## Coastal thermo-erosion in the Laptev Sea

F. Günther et al.

Title Page

Abstract

Introduction

Conclusions

References

Tables

Figures

◀

▶

◀

▶

Back

Close

Full Screen / Esc

Printer-friendly Version

Interactive Discussion



- Thieler, E. R., Himmelstoss, E. A., Zichichi, J. L., and Ergul, A.: Digital Shoreline Analysis System (DSAS) version 4.0 – an ArcGIS extension for calculating shoreline change, US Geological Survey Open-File Report 2008–1278, 2009. 2718
- Toutin, T.: Review article: geometric processing of remote sensing images: models, algorithms and methods, *Int. J. Remote Sens.*, 25, 1893–1924, doi:10.1080/0143116031000101611, 2004. 2714
- Treshnikov, A. F. (Ed.): Atlas Arktiki. (Atlas of the Arctic.), National Commission of Hydro-Meteorology and Environmental Protection, Major Dept. of Geodesy and Cartography, Moscow, 1985. 2710
- Ulrich, M., Morgenstern, A., Günther, F., Reiss, D., Bauch, K. E., Hauber, E., Rössler, S., and Schirrmeister, L.: Thermokarst in Siberian ice-rich permafrost: comparison to asymmetric scalloped depressions on Mars, *J. Geophys. Res.*, 115, E10009, doi:10.1029/2010JE003640, 2010. 2708
- Van Huissteden, J., Berrittella, C., Parmentier, F. J. W., Mi, Y., Maximov, T. C., and Dolman, A. J.: Methane emissions from permafrost thaw lakes limited by lake drainage, *Nat. Clim. Change*, 1, 119–123, doi:10.1038/nclimate1101, 2011. 2735
- Vasiliev, A. A., Streletskaia, I. D., Shirokov, R. S., and Oblogov, G. E.: Coastal permafrost evolution of western Yamal in context of climate change, *Kriosfera Zemli (Earth's Cryosphere)*, 15, 56–64, 2011. 2707, 2732
- Vonk, J. E., Sanchez-Garcia, L., van Dongen, B. E., Alling, V., Kosmach, D., Charkin, A., Semiletov, I. P., Dudarev, O. V., Shakhova, N., Roos, P., Eglinton, T. I., Andersson, A., and Gustafsson, Ö.: Activation of old carbon by erosion of coastal and subsea permafrost in Arctic Siberia, *Nature*, advance online publication, 489, 137–140, doi:10.1038/nature11392, 2012. 2736
- Wassmann, P.: Arctic marine ecosystems in an era of rapid climate change, *Prog. Oceanogr.*, 90, 1–17, doi:10.1016/j.pocean.2011.02.002, 2011. 2707
- Wetterich, S. and Schirrmeister, L.: Limnological studies in the Dmitrii Laptev Strait region, in: Russian–German Cooperation System Laptev Sea: The Expedition Lena – New Siberian Islands 2007 during the International Polar Year 2007/2008, edited by: Boike, J., Bolshiyarov, D. Y., Schirrmeister, L., and Wetterich, S., vol. 584, Reports on Polar and Marine Research, Alfred Wegener Institute, chap. 5.2, 155–163, 2008. 2715
- Wetterich, S., Schirrmeister, L., Andreev, A. A., Pudenz, M., Plessen, B., Meyer, H., and Kunitzky, V. V.: Eemian and Late Glacial/Holocene palaeoenvironmental records from permafrost

sequences at the Dmitry Laptev Strait (NE Siberia, Russia), *Palaeogeogr. Palaeoclimatol.*, 279, 73–95, doi:10.1016/j.palaeo.2009.05.002, 2009. 2713, 2718

Wetterich, S., Overduin, P. P., and Grigoriev, M. N. (Eds.): *Russian–German Cooperation System Laptev Sea: The Expedition Eastern Laptev Sea – Buor Khaya Peninsula 2010*, vol. 629, Reports on Polar and Marine Research, Alfred Wegener Institute, available at: <http://epic.awi.de/29931/>, 2011. 2717

Whitehouse, P. L., Allen, M. B., and Milne, G. A.: Glacial isostatic adjustment as a control on coastal processes: an example from the Siberian Arctic, *Geology*, 35, 747–750, doi:10.1130/G23437A.1, 2007. 2711

Winterfeld, M., Schirrmeister, L., Grigoriev, M. N., Kunitsky, V. V., Andreev, A., Murray, A., and Overduin, P. P.: Coastal permafrost landscape development since the Late Pleistocene in the western Laptev Sea, Siberia, *Boreas*, 40, 697–713, doi:10.1111/j.1502-3885.2011.00203.x, 2011.

2708

**BGD**

10, 2705–2765, 2013

## Coastal thermo-erosion in the Laptev Sea

F. Günther et al.

Title Page

Abstract

Introduction

Conclusions

References

Tables

Figures

◀

▶

◀

▶

Back

Close

Full Screen / Esc

Printer-friendly Version

Interactive Discussion



## Coastal thermo-erosion in the Laptev Sea

F. Günther et al.

**Table 1.** List of remote sensing data used for determination of coastline retreat along the coast of Mamontov Klyk and corresponding characteristics.

| Sensor     | Date<br>dd.mm.yyyy | Resolution ( $\delta_p$ )<br>[m] | RMSE ( $\delta_a$ & $\delta_r$ )<br>[m] | Orthorectification<br>basis | Observation<br>period |
|------------|--------------------|----------------------------------|---|-----------------------------|-----------------------|
| KH-4A AFT  | 27.07.1965         | 2.9                              | 2.05                                    | KH-4A DEM 1965              | long-term             |
| KH-4A AFT  | 27.07.1965         | 2.7                              | 2.9                                     | KH-4A DEM 1965              | long-term             |
| KH-4A AFT  | 27.07.1965         | 2.5                              | 4.42                                    | KH-4A DEM 1965              | long-term             |
| PRISM NDR  | 22.07.2009         | 2.5                              | 2.9                                     | PRISM DEM 2009              | long-term             |
| PRISM NDR  | 05.10.2009         | 2.5                              | 2.65                                    | PRISM DEM 2009              | long-term             |
| PRISM WIDE | 12.10.2007         | 2.5                              | 2.07                                    | Topomap DEM*                | long-term             |
| PRISM WIDE | 12.10.2007         | 2.5                              | 1.68                                    | PRISM DEM 2007              | short-term            |
| GeoEye-1   | 18.07.2009         | 0.5                              | 0.47                                    | GeoEye DEM 2011             | short-term            |
| GeoEye-1   | 01.08.2010         | 0.5                              | 1.75                                    | PRISM DEM 2007              | short-term            |
| KOMPSAT-2  | 13.08.2011         | 1.0                              | 0.82                                    | PRISM DEM 2007              | short-term            |
| GeoEye-1   | 09.08.2011         | 0.5                              | 1.16                                    | GeoEye DEM 2011             | short & long-term     |
| GeoEye-1   | 09.08.2011         | 0.5                              | 1.05                                    | GeoEye DEM 2011             | short & long-term     |
| RapidEye   | 29.07.2011         | 6.5                              | 3.18                                    | Topomap DEM*                | master                |
| RapidEye   | 09.08.2011         | 6.5                              | 3.93                                    | Topomap DEM*                | master                |

\* DEM based on topographic maps from ca. 1980 with an contour equidistance of 10 m (Grosse et al., 2006).

Title Page

Abstract

Introduction

Conclusions

References

Tables

Figures

◀

▶

◀

▶

Back

Close

Full Screen / Esc

Printer-friendly Version

Interactive Discussion



## Coastal thermo-erosion in the Laptev Sea

F. Günther et al.

**Table 2.** List of remote sensing and field data used for determination of coastline retreat along the west coast of the Buor Khaya Peninsula and corresponding characteristics.

| Sensor          | Date<br>dd.mm.yyyy | Resolution ( $\delta_p$ )<br>[m] | RMSE ( $\delta_a$ & $\delta_r$ )<br>[m] | Orthorectification<br>basis | Observation<br>period |
|-----------------|--------------------|----------------------------------|---|-----------------------------|-----------------------|
| KH-4B AFT       | 24.07.1969         | 2.0                              | 1.38                                    | Topomap DEM 1973            | long-term             |
| KH-4B AFT       | 24.07.1969         | 2.0                              | 1.94                                    | Topomap DEM 1973            | long-term             |
| SPOT-5 HRV      | 08.10.2011         | 2.5                              | 1.08                                    | SPOT-5 DEM 2012             | long-term             |
| SPOT-5 HRV      | 08.10.2011         | 2.5                              | 2.27                                    | SPOT-5 DEM 2012             | long-term             |
| GeoEye-1        | 13.07.2009         | 0.5                              | 0.91                                    | SPOT-5 DEM 2012             | short-term            |
| GeoEye-1        | 13.07.2009         | 0.5                              | 1.17                                    | SPOT-5 DEM 2012             | short-term            |
| GeoEye-1        | 18.07.2011         | 0.5                              | 0.87                                    | GeoEye DEM 2011             | short-term            |
| Geodetic survey | 05.–17.08.2010     | –                                | 1.2–1.5                                 | –                           | short-term            |
| RapidEye        | 08.08.2010         | 6.5                              | 4.04                                    | Topomap DEM 1973            | master dataset        |

Title Page

Abstract

Introduction

Conclusions

References

Tables

Figures

◀

▶

◀

▶

Back

Close

Full Screen / Esc

Printer-friendly Version

Interactive Discussion



## Coastal thermo-erosion in the Laptev Sea

F. Günther et al.

**Table 3.** List of remote sensing data used for determination of coastline retreat along Oyogos Yar coast (Dmitry Laptev Strait) and corresponding characteristics.

| Sensor     | Date<br>dd.mm.yyyy | Resolution ( $\delta_p$ )<br>[m] | RMSE ( $\delta_a$ & $\delta_r$ )<br>[m] | Orthorectification<br>basis | Observation<br>period |
|------------|--------------------|----------------------------------|---|-----------------------------|-----------------------|
| KH-4A AFT  | 26.06.1968         | 2.9                              | 3.57                                    | sea & mean cliff top level  | long-term             |
| KH-4A AFT  | 26.06.1968         | 2.7                              | 4.78                                    | sea & mean cliff top level  | long-term             |
| SPOT-5 HRV | 09.10.2011         | 2.5                              | 2.87                                    | SPOT-5 DEM 2011             | long-term             |
| KOMPSAT-2  | 25.09.2009         | 1.0                              | 1.01                                    | sea & mean cliff top level  | short-term            |
| KOMPSAT-2  | 04.08.2011         | 1.0                              | 2.94                                    | sea & mean cliff top level  | short-term            |
| RapidEye   | 20.08.2010         | 6.5                              | 6.89                                    | Topomap DEM*                | master & long-term    |
| RapidEye   | 26.08.2010         | 6.5                              | 3.51                                    | Topomap DEM*                | master                |

\* Santoro and Strozzi (2012)

Title Page

Abstract

Introduction

Conclusions

References

Tables

Figures



Back

Close

Full Screen / Esc

Printer-friendly Version

Interactive Discussion



## Coastal thermo-erosion in the Laptev Sea

F. Günther et al.

**Table 4.** List of mean coastal erosion rates attributable to thermo-denudation and abrasion, standard deviations and NDTI, evaluated across all transects.

|                                    | long-term observations | long- and short-term observations | short-term observations |
|------------------------------------|------------------------|-----------------------------------|-------------------------|
| <i>N</i> of transects              | 3635                   | 824                               | 824                     |
| mean TD rate [ $\text{m a}^{-1}$ ] | -2.2                   | -3.3                              | -5.3                    |
| St.dev. TD                         | 1.55                   | 1.27                              | 2.78                    |
| mean TA rate [ $\text{m a}^{-1}$ ] | -1.9                   | -3.3                              | -5.7                    |
| St.dev. TA                         | 1.49                   | 1.22                              | 3.17                    |
| NDTI                               | 0.07                   | 0.003                             | -0.04                   |

Title Page

Abstract

Introduction

Conclusions

References

Tables

Figures

◀

▶

◀

▶

Back

Close

Full Screen / Esc

Printer-friendly Version

Interactive Discussion



## Coastal thermo-erosion in the Laptev Sea

F. Günther et al.

**Table 5.** Total organic-carbon (TOC) flux that result from the erosion observed in the Laptev Sea region. Values are separated by site (Mamontov Klyk, Buor Khaya, Oyogos Yar) and, within each site, by yedoma and thermokarst depression (alas).

|  | Mamontov Klyk          |                        | Buor Khaya              |                        | Oyogos Yar              |                        |
|--|------------------------|------------------------|-------------------------|------------------------|-------------------------|------------------------|
|  | yedoma                 | alas                   | yedoma                  | alas                   | yedoma                  | alas                   |
| <i>N</i> of transects                                | 880                    | 241                    | 293                     | 660                    | 272                     | 1289                   |
| erosion (TD + TA) [ma <sup>-1</sup> ]                | -2.13                  | -1.84                  | -0.85                   | -0.38                  | -2.85                   | -3.38                  |
| mean cliff height [m]                                | 16.5                   | 4                      | 22.5                    | 10.5                   | 23                      | 10                     |
| eroded volume [m <sup>3</sup> ]                      | 1.54 × 10 <sup>6</sup> | 0.09 × 10 <sup>6</sup> | 0.28 × 10 <sup>6</sup>  | 0.13 × 10 <sup>6</sup> | 0.89 × 10 <sup>6</sup>  | 2.18 × 10 <sup>6</sup> |
| uncertainty [m <sup>3</sup> ]                        | ±9 × 10 <sup>3</sup>   | ±1 × 10 <sup>3</sup>   | ±4 × 10 <sup>3</sup>    | ±6 × 10 <sup>3</sup>   | ±12 <sup>3</sup>        | ±23 × 10 <sup>3</sup>  |
| mean TOC [kgm <sup>-3</sup> ]                        | 21.8 <sup>a</sup>      | 23.1 <sup>a</sup>      | 13.4 <sup>b</sup>       | 19.9 <sup>b</sup>      | 17.6 <sup>a</sup>       | 28.1 <sup>a</sup>      |
| St. Dev. ( <i>n</i> )                                | ±9.1 (31) <sup>a</sup> | ±7.2 (4) <sup>a</sup>  | ±11.0 (47) <sup>b</sup> | ±9.6 (34) <sup>b</sup> | ±13.3 (18) <sup>a</sup> | ±6.3 (5) <sup>a</sup>  |
| estimated ice wedge vol. [%]                         | 50 <sup>a</sup>        | 10 <sup>a</sup>        | 50 <sup>b</sup>         | 10 <sup>b</sup>        | 50 <sup>a</sup>         | 10 <sup>a</sup>        |
| corrected TOC [kgm <sup>-3</sup> ] <sup>c</sup>      | 10.92                  | 20.81                  | 6.73                    | 17.91                  | 8.79                    | 25.25                  |
| uncertainty [kgm <sup>-3</sup> ] <sup>c</sup>        | 4.5                    | 6.5                    | 5.5                     | 8.6                    | 6.7                     | 5.7                    |
| total annual carbon flux [t]                         | 16 × 10 <sup>3</sup>   | 1.8 × 10 <sup>3</sup>  | 1.9 × 10 <sup>3</sup>   | 2.3 × 10 <sup>3</sup>  | 7.8 × 10 <sup>3</sup>   | 55 × 10 <sup>3</sup>   |
| uncertainty [t]                                      | ±8 × 10 <sup>3</sup>   | ±0.1 × 10 <sup>3</sup> | ±1.7 × 10 <sup>3</sup>  | ±1.3 × 10 <sup>3</sup> | ±6.8 × 10 <sup>3</sup>  | ±17 × 10 <sup>3</sup>  |
| annual flux<br>per km coastline [tkm <sup>-1</sup> ] | 380                    | 150                    | 130                     | 70                     | 570                     | 850                    |
|  |                        | 330                    |                         | 88                     |                         | 800                    |

<sup>a</sup> Schirrneister et al. (2011b);

<sup>b</sup> unpublished data, Strauss (2013);

<sup>c</sup> calculated following Strauss et al. (2012).

Title Page

Abstract

Introduction

Conclusions

References

Tables

Figures

◀

▶

◀

▶

Back

Close

Full Screen / Esc

Printer-friendly Version

Interactive Discussion



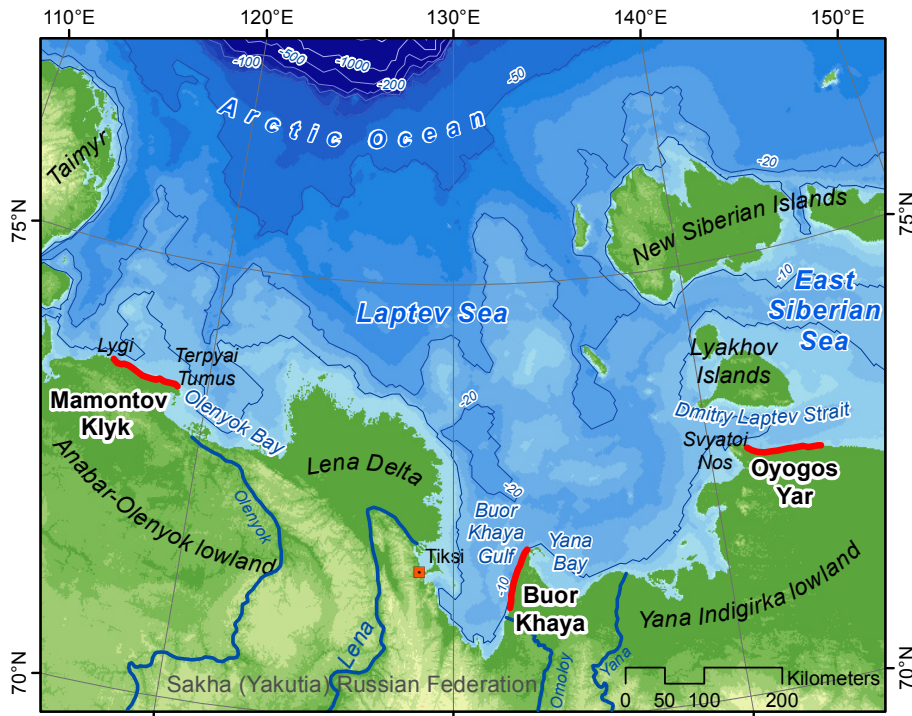


**Fig. 1.** Location of the study sites within the Laptev Sea region. Analyzed coastline sections are marked as red lines and comprise from west to east: Mamontov Klyk, Buor Khaya and Oyogos Yar.

## BGD

10, 2705–2765, 2013

### Coastal thermo-erosion in the Laptev Sea

F. Günther et al.

Title Page

Abstract

Introduction

Conclusions

References

Tables

Figures



Back

Close

Full Screen / Esc

Printer-friendly Version

Interactive Discussion



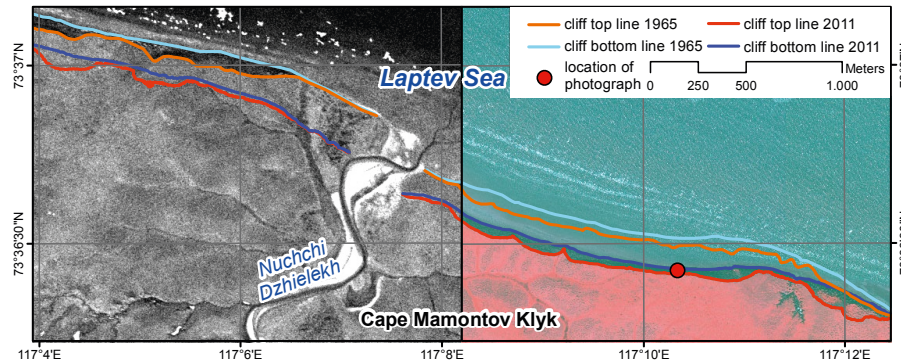
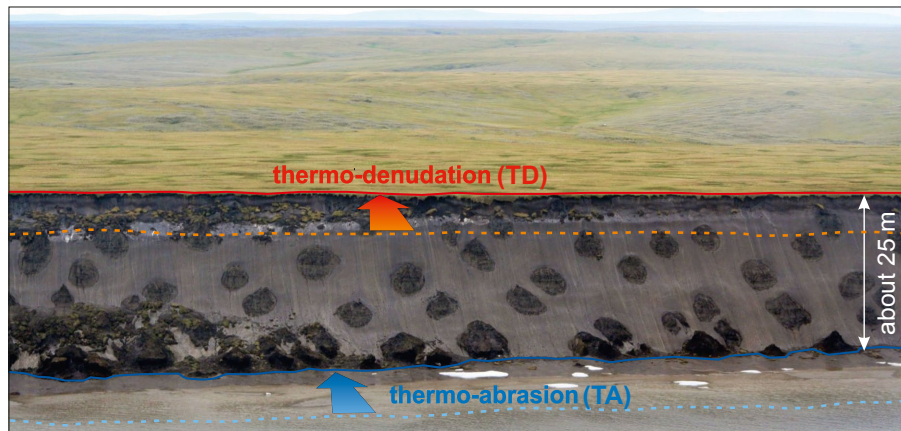


**Fig. 2.** Upper graphic: delineation of thermo-denudation (TD) and thermo-abrasion (TA) based on the example of a 25 m high yedoma coast composed of Ice Complex deposits in the western Laptev Sea between Cape Mamontov Klyk and Nuchchi Dzhiielekh River mouth (photograph taken from helicopter, courtesy of H.-W. Hubberten); Lower graphic: the same section displayed with multitemporal planimetric coastline positions in GIS (lower left: 1965 Corona KH-4A imagery as background; lower right: 2011 GeoEye imagery displayed as false color infrared composite).

**Coastal thermo-erosion in the Laptev Sea**

F. Günther et al.

Title Page

Abstract

Introduction

Conclusions

References

Tables

Figures

◀

▶

◀

▶

Back

Close

Full Screen / Esc

Printer-friendly Version

Interactive Discussion



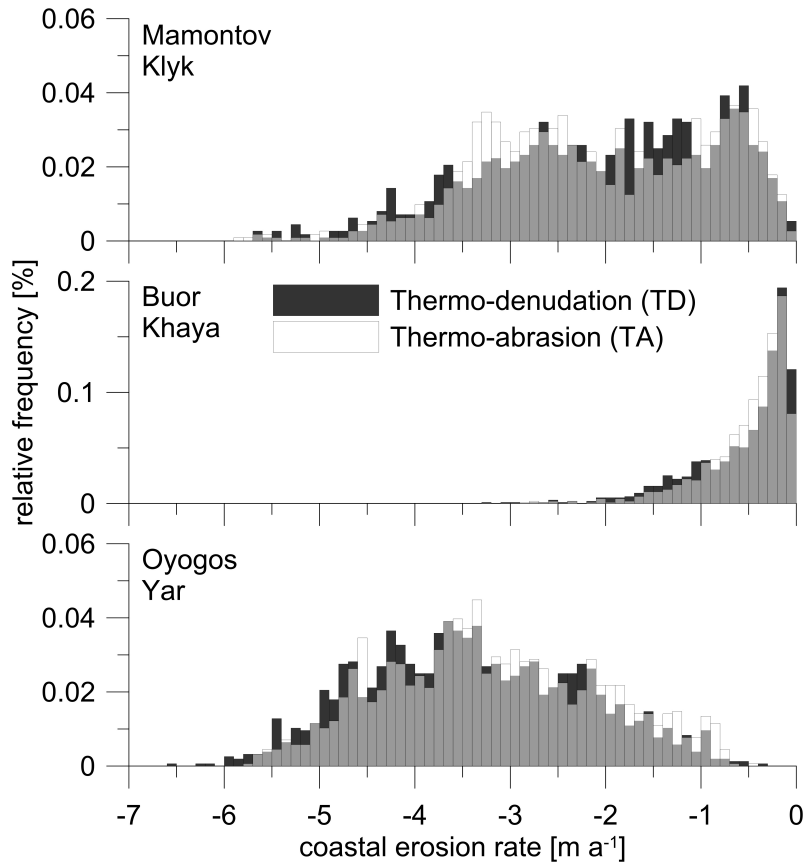


**Fig. 3.** Site specific histograms of long-term mean annual coastal erosion rates ( $\text{m a}^{-1}$ ) obtained from coastal transect data, separated into thermo-denudation (TD) and thermo-abrasion (TA) rates.

[Title Page](#)

[Abstract](#)

[Introduction](#)

[Conclusions](#)

[References](#)

[Tables](#)

[Figures](#)

[◀](#)

[▶](#)

[◀](#)

[▶](#)

[Back](#)

[Close](#)

[Full Screen / Esc](#)

[Printer-friendly Version](#)

[Interactive Discussion](#)



## Coastal thermo-erosion in the Laptev Sea

F. Günther et al.

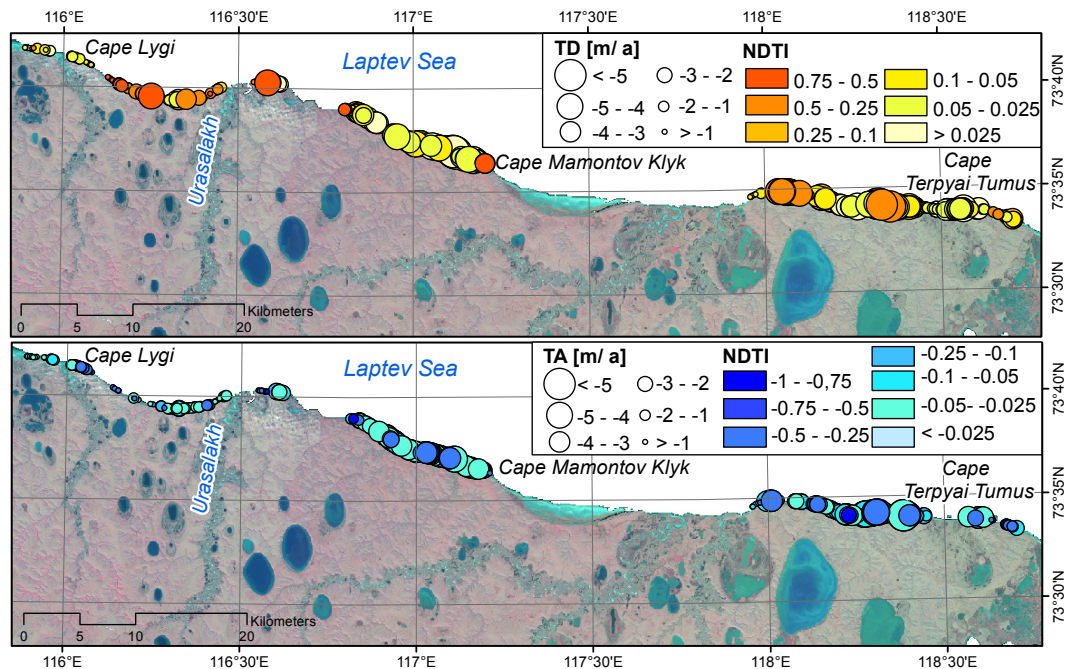


**Fig. 4.** Thematic map of coastal thermo-erosion transect data along the studied coastline of Mamontov Klyk (Anabar–Olenyok lowland). The upper map segment illustrates color coded positive NDTI values associated with prevailing thermo-denudation (TD), the lower map illustrates color coded negative NDTI values associated with prevailing thermo-abrasion (TA). The symbol size is equivalent to erosion values.

Title Page

Abstract

Introduction

Conclusions

References

Tables

Figures

⏪

⏩

◀

▶

Back

Close

Full Screen / Esc

Printer-friendly Version

Interactive Discussion



## Coastal thermo-erosion in the Laptev Sea

F. Günther et al.

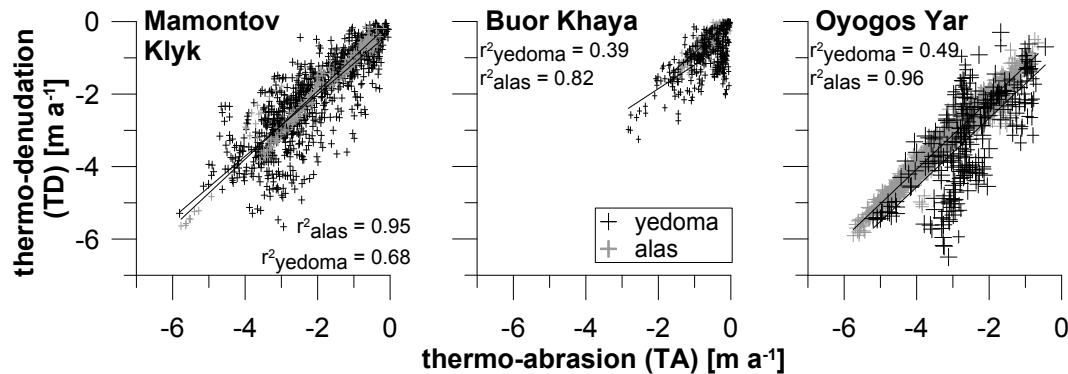


**Fig. 5.** Mean annual thermo-denudation (TD) vs. thermo-abrasion (TA) rates, divided into alas and yedoma coastline types by study sites. Cross symbols are built of error bars of TD and TA rate uncertainty (see Sect. 3.5), corresponding to the TD and TA axis, respectively.

Title Page

Abstract

Introduction

Conclusions

References

Tables

Figures

◀

▶

◀

▶

Back

Close

Full Screen / Esc

Printer-friendly Version

Interactive Discussion



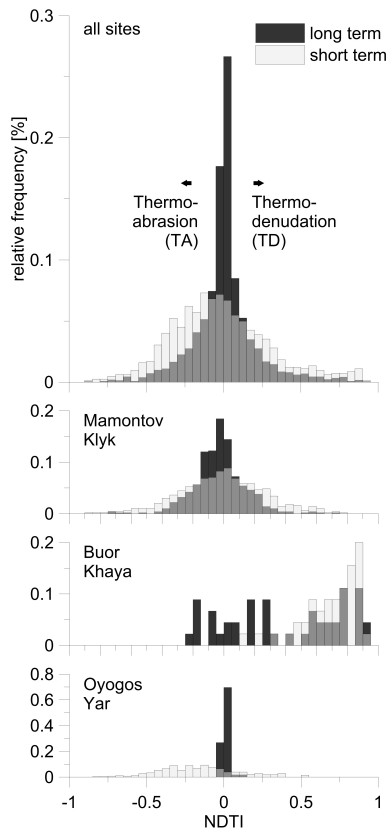


**Fig. 6.** Histograms of Normalized Difference Thermo-erosion Index (NDTI) values for the two time periods of observation are shown (from top to bottom) for the three coastal study sites considered as a whole and separately for Mamontov Klyk, Buor Khaya, and Oyogos Yar. Negative NDTI values indicate prevailing thermo-abrasion (TA), positive NDTI values thermo-denudation (TD).

## Coastal thermo-erosion in the Laptev Sea

F. Günther et al.

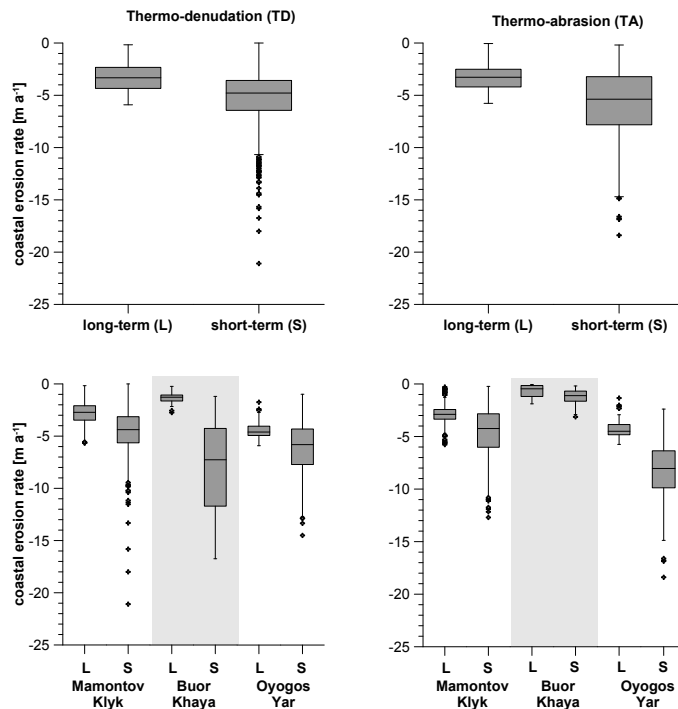


**Fig. 7.** Box plots of the thermo-erosion rates for long-term (39 to 43 yr) and short-term measurements (last 1 to 4 yr). Upper graphs: distribution of all TD (upper left) and TA (upper right) measurements ( $n = 3635$ ), for long and short-term periods. Lower graphs: distribution of off all thermo-denudation (TD; lower left) and thermo-abrasion (TA, lower right) measurements from transects, for which both long and short-term observations are available, plotted separately by study sites Mamontov Klyk, Buor Khaya, and Oyogos Yar. Box plots show lower and upper quartiles, medians and outliers (points), defined as erosion rates more than 1.5 times the interquartile range above or below the median.

Title Page

Abstract

Introduction

Conclusions

References

Tables

Figures

◀

▶

◀

▶

Back

Close

Full Screen / Esc

Printer-friendly Version

Interactive Discussion



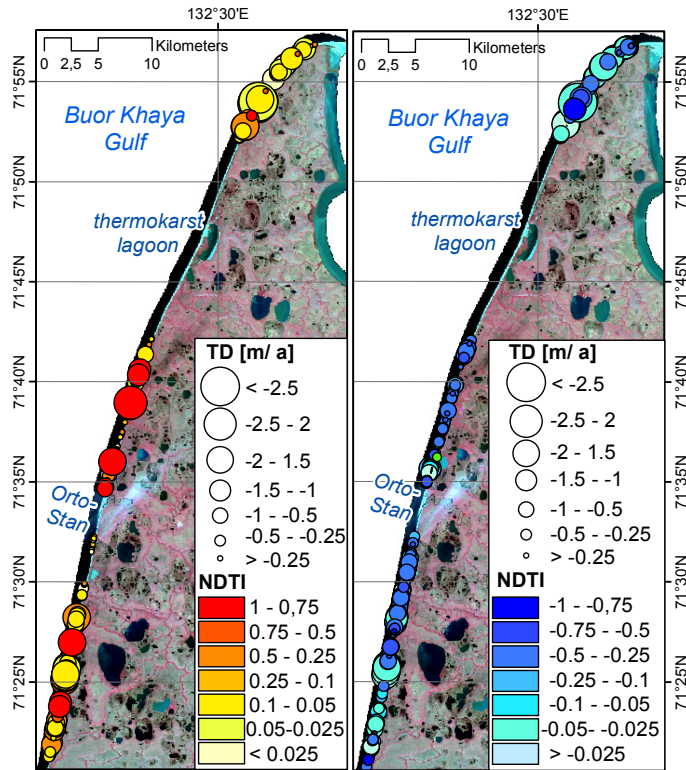


**Fig. 8.** Thematic map of coastal thermo-erosion transect data along the studied coastline of Buor Khaya (west coast of the Buor Khaya Peninsula). The left map segment illustrates color coded positive NDTI values associated with prevailing thermo-denudation (TD), the right map segment illustrates color coded negative NDTI values associated with prevailing thermo-abrasion (TA). The symbol size is equivalent to erosion values.

## Coastal thermo-erosion in the Laptev Sea

F. Günther et al.

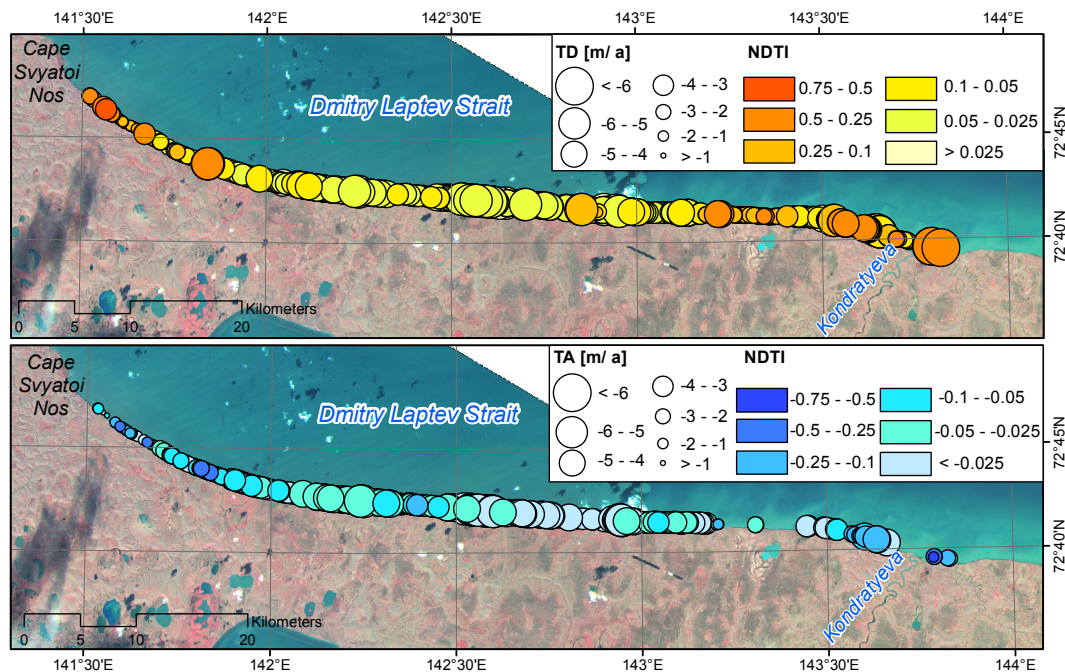


**Fig. 9.** Thematic map of coastal thermo-erosion transect data along the studied coastline of Oyogos Yar (Yana-Indigirka lowland west of Cape Svyatoi Nos; Dmitry Laptev Strait). The upper map segment illustrates color coded positive NDTI values associated with prevailing thermo-denudation (TD), the lower map illustrates color coded negative NDTI values associated with prevailing thermo-abrasion (TA). The symbol size is equivalent to erosion values.

Title Page

Abstract

Introduction

Conclusions

References

Tables

Figures

◀

▶

◀

▶

Back

Close

Full Screen / Esc

Printer-friendly Version

Interactive Discussion

